Titre: Title:	Dynamics of Differential Drive Wheel Mobile Robot with Free Caster Wheels
Auteur: Author:	Mohammadreza Montazerijouybari
Date:	2022
Type:	Mémoire ou thèse / Dissertation or Thesis
Référence: Citation:	Montazerijouybari, M. (2022). Dynamics of Differential Drive Wheel Mobile Robot with Free Caster Wheels [Master's thesis, Polytechnique Montréal]. PolyPublie. https://publications.polymtl.ca/10216/

URL de PolyPublie: PolyPublie URL:	https://publications.polymtl.ca/10216/
Directeurs de recherche: Advisors:	Luc Baron, & Sousso Kelouwani
Programme: Program:	Génie mécanique

POLYTECHNIQUE MONTRÉAL
affiliée à l'Université de Montréal

Dynamics of Differential Drive Wheel Mobile Robot with Free Caster Wheels

MOHAMMADREZA MONTAZERIJOUYBARI
Département de génie mécanique

Mémoire présenté en vue de l'obtention du diplôme de *Maîtrise ès sciences appliquées*
Génie mécanique

Janvier 2022

POLYTECHNIQUE MONTRÉAL
affiliée à l'Université de Montréal

Ce mémoire intitulé :

Dynamics of Differential Drive Wheel Mobile Robot with Free Caster Wheels

présenté par **Mohammadreza MONTAZERIJOUYBARI**
en vue de l'obtention du diplôme de *Maîtrise ès sciences appliquées*
a été dûment accepté par le jury d'examen constitué de :

René MAYER, président
Luc BARON, membre et directeur de recherche
Sousso KELOUWANI, membre et codirecteur de recherche
Abolfazl MOHEBBI, membre

DEDICATION

To my beautiful wife and my family who never wavered in their support . . .

ACKNOWLEDGEMENTS

I would like to express my deepest appreciation to my supervisor Prof. Luc Baron for his valuable advice, time and effort. Also, I would like to extend my sincere thanks to Prof. Sousso Kelouwani provided me with encouragement and patience throughout the duration of this study. Moreover, I am grateful to Prof. René Mayer and Prof. Abolfazl Mohebi for kindly accepting to participate in this jury.

RÉSUMÉ

Les véhicules à guidage automatique (AGV) sont utilisés dans les lignes de production et les entrepôts pour transporter des marchandises sur des chemins prédéterminés. Cependant, la nécessité d'utiliser des AGV en libre parcours dans les sentiers intérieurs augmente récemment. Un AGV à portée libre est appelé Robot Mobile Autonome (AMR) qui a des capacités de prise de décision comme l'évitement d'objets ou la planification de trajectoire. Pour un tel robot, le suivi de la trajectoire prévue, précisément, est important.

L'une des configurations les plus courantes de l'AMR consiste en deux roues motrices différentielles et des roues pivotantes qui offre une bonne stabilité et maniabilité. D'une part, ces roues augmentent la stabilité du robot en suivant passivement la trajectoire dictée des roues motrices tout en supportant une charge verticale. D'autre part, les rover pivotauto sont la principale source d'incertitude qui entraînent une augmentation de l'erreur de suivi de trajectoire. De plus, le chargement et le déchargement d'un robot avec une charge inconnue, mais dans une plage prédéterminée, modifie le centre de masse (COM) du robot, ce qui entraînent davantage d'erreurs de suivi de trajectoire.
Dans cette mémoire, nous étudions dans un premier temps le comportement des rover pivotauto au niveau cinématique et nous perposons un modèle cinématique pour prédire son orientation dans certaines circonstances. Ensuite, le modèle dynamique d'un AMR avec la variable COM est considéré. En outre, la mise en œuvre de capteurs de force est proposée pour mesurer les forces d'interaction avec le sol des roues et déterminer l'emplacement du COM. Par la suite, une méthode de contrôle non linéaire a été utilisée pour traiter le nouveau modèle cinématique et dynamique.
Les performances du modèle proposé ont été testées dans un environnement de simulation du nouveau modèle par rapport à un modèle existant qui considère le COM fixe sans aucun retour de force. Les résultats ont montrés une amélioration significative des performances et une baisse de l'erreur de suivi de trajectoire.

ABSTRACT

Automated Guided Vehicles (AGVs) are used in production lines and warehouses to carry merchandises in predetermined paths. However, necessity of using free range AGVs in indoor paths is raising recently. A free range AGV is called Autonomous Mobile Robot (AMR) which has decision making abilities like object avoidance or path planing. For such a robot, the tracking of the planned path, precisely, is more important.

One of the most common configuration of AMR consists of two differential drive wheels and caster wheels which offers good stability and maneuverability. On one hand, Caster wheels allow the robot to follow dictated paths of the driving wheels passively while carrying vertical load. On the other hand, caster wheels are the main source of uncertainty which cause increase in path tracking error. Moreover, loading and unloading a robot with an unknown load, but in a predetermined range, changes the robot's Center Of Mass (COM) which cause more path tracking error.

In this thesis, we study the behaviour of caster wheels in kinematic level and we proposed a kinematic model to predict its orientation in certain circumstances. Then, the kinematic model and the dynamic model of an AMR with variable COM was considered. The addition of force sensors has been proposed in order to measure the wheel ground interaction forces and to determine the location of COM. Afterwards, some nonlinear control method was used to deal with new kinematic and dynamic models.

The performance of the proposed model was tested in simulation environment. The results of the new model compared with an existing model which considers fixed COM without any force feedback. The results have shown significant improvement in performance and a drop in path tracking errors.

TABLE OF CONTENTS

LIST OF TABLES

LIST OF FIGURES

LIST OF SYMBOLS AND ACRONYMS

AMR	Autonomous Mobile Robot
AGV	Automated Guided Vehicle
COM	Center Of Mass
ICOM	Instantaneous Center Of Mass
ICOR	Instantaneous Center Of Rotation
IMU	Inertia Measurement Unit
NS	Navigation System
DDWMR	Differential Drive Wheel Mobile Robot
FF	Force Feedback
$\mathcal{F}$	Base Frame
$\mathcal{M}$	Moving Frame
o'	Origin of the frame $\mathcal{M}$
$\mathbf{z}$	Vertical axis of frames $\mathcal{F}$ and $\mathcal{M}$
$\mathbf{h}$	Longitudinal axis of the frame $\mathcal{M}$
$\mathbf{l}$	lateral axis of the frame$\mathcal{M}$
p_1	Right driving wheel contact point with the ground
p_2	Left driving wheel contact point with the ground
c_1	Center of the right driving wheel
c_1	Center of the left driving wheel
$\dot{\theta}_1$	Angular Velocity of the right driving wheel
$\dot{\theta}_2$	Angular Velocity of the left driving wheel
r	Driving wheel radius
ϕ	Platform orientation
$\dot{\phi}$	Angular velocity of the platform
v	heading velocity of the platform along $\mathbf{h}$-axis
$\mathbf{v}$	Twist of differential drive wheel platform in the frame $\mathcal{M}$
$\dot{\mathbf{q}}$	Twist of differential drive wheel platform in the frame $\mathcal{F}$
δ_1	Slippage angle of right driving wheel
δ_2	Slippage angle of left driving wheel
ϵ	Skidding distance of the platform
$\mathbf{R}(\phi)$	Rotation matrix of the frame $\mathcal{M}$ with respect to the frame $\mathcal{F}$
$\mathbf{J}$	Jacobin of a differential drive wheel platform
c	Instantaneous center of mass point

a	Distance of ICOM point from the origin of the frame $\mathcal{M}$ along **h**-axis
b	Distance of ICOM point from the origin of the frame $\mathcal{M}$ along **l**-axis
$\mathbf{J}_c$	Jacobin of an AMR
v_c	Heading velocity of an AMR along **h**-axis
$\mathbf{v}_c$	Twist of AMR in the frame $\mathcal{M}$
$\dot{\mathbf{q}}_c$	Twist of AMR in the frame $\mathcal{F}$
e	Off center distance of the caster wheel pivot point
c_r	ICOR point
ψ_1	Orientation of the front right caster wheel with respect to the **h**-axis
ψ_2	Orientation of the front left caster wheel with respect to the **h**-axis
ψ_3	Orientation of the rear right caster wheel with respect to the **h**-axis
ψ_4	Orientation of the rear right caster wheel with respect to the **h**-axis
α_1	The angle between the **h**-axis and the line connecting front right caster wheel pivot point and ICOR point
α_2	The angle between the **h**-axis and the line connecting front left caster wheel pivot point and ICOR point
α_3	The angle between the **h**-axis and the line connecting rear right caster wheel pivot point and ICOR point
α_4	The angle between the **h**-axis and the line connecting rear left caster wheel pivot point and ICOR point
h_1	The perpendicular distance between the pivot point of front caster wheels with the **l**-axis
h_2	The perpendicular distance between the pivot point of rear caster wheels with the **l**-axis
f	The perpendicular distance between the pivot point of caster wheels with the **h**-axis
s	The perpendicular distance between the ICOR point with the **h**-axis
r_c	Caster wheel radius
$\dot{\mathbf{t}}$	Twist of AMR
$\dot{\mathbf{t}}_1$	Twist of the right driving wheel
$\dot{\mathbf{t}}_2$	Twist of the left driving wheel
$\dot{\mathbf{t}}_3$	Twist of the platform including weight excluding caster wheels
$\mathbf{T}$	Twist shaping matrix of AMR
$\mathbf{T}_1$	Twist shaping matrix of the right driving wheel
$\mathbf{T}_2$	Twist shaping matrix of the left driving wheel
$\mathbf{T}_3$	Twist shaping matrix of the platform including weight

$\mathbf{M}$	Mass matrix of AMR
$\mathbf{M}_1$	Mass matrix of the right driving wheel
$\mathbf{M}_2$	Mass matrix of the left driving wheel
$\mathbf{M}_3$	Mass matrix of the platform including weight excluding casters
$\mathbf{I}_1$	Inertia matrix of the right driving wheel
$\mathbf{I}_2$	Inertia matrix of the left driving wheel
$\mathbf{I}_3$	Inertia matrix of the platform including weight excluding caster wheels
$\mathbf{W}$	Angular velocity matrix of AMR
$\mathbf{W}_1$	Angular velocity matrix of the right driving wheel
$\mathbf{W}_2$	Angular velocity matrix of the left driving wheel
$\mathbf{W}_3$	Angular velocity matrix of the platform including weight excluding caster wheels
$\mathbf{\Omega}_1$	Cross product matrix of the angular velocity vector of the right driving wheel
$\mathbf{\Omega}_2$	Cross product matrix of the angular velocity vector of the left driving wheel
$\mathbf{\Omega}_3$	Cross product matrix of the angular velocity vector of the platform
$\mathbf{w}^A$	Driving force vector of AMR
$\mathbf{w}_1^A$	Driving force vector of the right driving wheel
$\mathbf{w}_2^A$	Driving force vector of the left driving wheel
$\mathbf{w}_3^A$	Driving force vector of the platform
$\mathbf{w}^D$	Dissipative force vector of AMR
$\mathbf{w}_1^D$	Dissipative force vector of the right driving wheel
$\mathbf{w}_2^D$	Dissipative force vector of the left driving wheel
$\mathbf{w}_3^D$	Dissipative force vector of the platform
$\mathbf{q}_r$	Reference pose
$\mathbf{q}_d$	Feedback pose
$\mathbf{e}_q$	Pose error
$\mathbf{q}_{\dot{r}}$	Reference twist
$\mathbf{q}_{\dot{d}}$	Feedback twist
v_r	Reference heading velocity in the frame $\mathcal{M}$
$\mathbf{e}_{\dot{q}}$	Twist error
$\dot{\mathbf{q}}_c$	Input pose
$\ddot{\mathbf{q}}_c$	Time-derivative of input pose
τ_1	Right driving wheel input torque
τ_2	Left driving wheel input torque

$s(t)$	Sliding surface
$\dot{s(t)}$	Time-derivative of the sliding surface
k_1	Back-stepping control coefficient
k_2	Back-stepping control coefficient
k_3	Back-stepping control coefficient
k_4	Coefficient of the sliding surface
k_5	Coefficient of the switching control

LIST OF APPENDICES

CHAPTER 1 INTRODUCTION

1.1 Problem Statement

Automated Guided Vehicles (AGVs) are used in industries to supply parts and sub assemblies to the production lines. Among various mobile robot configurations, the combination of caster wheel and differential drive wheels is the most common type offering good stability and maneuverability. Also, the necessity of replacing AGVs by Autonomous Mobile Robots (AMRs) is raising recently because AMRs are smarter and more flexible than AGVs. AMRs do not require fixed routes and they are able to move out of the way of obstacles independently. However, applying unknown weight (but in an acceptable range) on an AMR negatively affects robot performance by increasing path tracking error.
The unknown load changes robot's Center Of Mass (COM) as well as wheels ground interaction forces. The eccentricity of COM affects the precision of dynamic model and consequently kinematic model. Furthermore, caster wheels apply not only unknown dissipative forces to the robot's body, but also the dissipative force's direction changes and produce a large amount of uncertainty on the control system. Since the amount of dissipative force is unknown, the angle between caster wheel and robot body estimated in literature [1] and [2] will not help to tackle with the problem. Moreover, the variations in friction between wheels and ground surface, affect the caster wheel ground interaction force and cause more uncertainty. The amount of uncertainty caused by COM variation and caster wheel's dissipative force, lead to an unacceptable range of path tracking error.

1.2 Research Question

Applying an unknown weight on an AMR cause undesirable path tracking error. The aim of this research is to decrease the path tracking error of an AMR with variable COM which has special configuration and dimensions ordered by an industrial company. The main research question is:

- Is it possible to decrease path tracking error of an autonomous mobile robot having a variable center of mass?

1.3 Objectives

The aim of this study is to drive a new kinematic and dynamic model for an AMR with variable COM to reduce its path tracking error. Since the location of COM is varying, the kinematic model which yields the velocity of COM has to be derived first. Additionally, the kinematic of the caster wheels, installed on an differential drive wheel mechanism, has been considered. Then, the dynamic model was reconsidered based on the location of instantaneous COM. Moreover, the implementation of force sensors to determine the position of COM and to measure dissipative force of wheels was proposed. In order to be able to evaluate the proposed method, a simulation environment including physics engine to simulate wheel ground interaction forces was chosen. Finally, the robot model with actual dimensions was imported to chosen simulator and the performance of proposed method was compared with the other latest method.

1.4 Assumption

The following assumptions has been made to simulate this problem:

- Since the robot does not demand to tackle with high speed maneuver, the pure rolling situation assumed for both driving wheels and caster wheels.
- The robot has planar motion in a smooth flat rigid surface with fixed friction coefficient.
- Although the friction between wheels and ground has considered at any kind in simulation but, the robot body and wheels are considered as rigid.

1.5 Organization of the thesis

Chapter 2 presents a literature review on the kinematics of AMR, in particular with caster wheels. It also discuses the dynamics and control of these vehicles with regard to a varying COM.
Chapter 3 presents a kinematic model of an AMR with caster wheels which has been the subject of a conference paper [1]. The new kinematic model adds kinematics of a caster wheel to a usual kinematic model of an AMR in the aim of take casters' dissipative force into account.
Chapter 4 presents the kinematics and dynamics of an AMR with variable COM. Furthermore, the main idea of this thesis to answer the research question is proposed.
Chapter 5 explains the control method which was used to deal with the nonholonomic nature

of the AMR and the new kinematic and dynamic models. Furthermore, the simulation result of the new dynamic model with variable COM is compered by the previous dynamic model based on fixed COM.

Chapter 6 briefly concludes the works done trough this thesis and discuses the limitations of the job and finally provides some ideas for future works.

CHAPTER 2 LITERATURE REVIEW

2.1 Caster wheel orientation

Caster wheels could be divide into two main categories namely, powered casters and unpowered casters. Powered casters are equipped with two motors which one motor rotates the wheel around the horizontal axis, while the other one rotates the wheel around the vertical axis. Opposed to the powered caster wheels, unpowered caster wheels follow the path dictated by driving wheels, meanwhile carrying the normal load of the base. In this study, we focused on unpowered casters and wherever we name a caster wheel in this thesis, we mean unpowered casters.

Casters are designed in such a way that do not resist against rolling and turning. Whoever, when it comes to carrying a load, specially in a free range robot, the uncertainty originated from casters are not negligible. Having said that, the resistance force caused by caster wheels as an uncertainty, is not necessarily along the moving direction of the robot. Consider a robot with two caster wheels in arbitrary direction, When the robot start moving, casters gradually rotates to the direction of the robot. After some time, the casters' orientation remains alongside the robot's moving direction. The period when a caster wheel turns towards the robot's moving direction, is called transition mode. Caster wheels orientation after transition mode have studied in literature [2]. Wu et al, showed that when the robot is turning along an Instantaneous Center of Rotation (ICOR), the velocity of caster wheels' pivot points is normal to the line connecting Caster's pivot point and ICOR. The situation discussed in [2] is the orientation of caster wheel right after transition mode. This will be discussed in details in chapter 3.

Another important application of caster wheel is to help to stabilize wheelchairs. In [3], Chénier et al, derived an estimator to estimate the orientation of caster wheels in a wheelchair. The estimated angle of so called estimator fluctuates around the real value and after a while the error value converges to zero. The geometrical behaviour of caster wheel in transition mode remained some how pristine.

2.2 Control method

Many AMRs are composed of two differential driving wheels and from two to four caster wheels for stabilization. Although, the number and location of caster wheel do not affect the control method, the amount of uncertainty caused by caster wheels affect the whole con-

trol system's performance. Considering the differential drive mechanism stabilized by caster wheels, the most challenging part of the control system is to deal with the non-linearity of the system. This non-linearity is inherited from nonholonomic property of the system originated from kinematic constrains. Because of the kinematics constrains, the robot cannot have a lateral motion and considered to be skid free. The kinematic constrains of the robot prevents the control system to use integration of velocities for localization. In other words, according to Brockett's conditions, the non linearity of the problem which is inherited from nonholonomic kinematic constrains, cannot be dealt with continuous time invariant feedback controller.

Many litterateurs have proposed different methods to deal with nonholonomic properties of differential drive wheel robot for path tracking in presence of uncertainty in kinematic level. Although these methods makes the robot follow the required path and were exponentially stable, all the applied nonlinear control methods were in kinematic level [4–7]. These methods took the advantage of back-stepping, sliding mode and adaptive control but were not sufficient to address the uncertainties caused in dynamic level. Approaches applying nonlinear control methods considering dynamic model were developed later [8–11]. Feedback linearization were the next purposed solution to tackle with the challenge of nonholonomic properties of differential drive wheel mobile robot [12]. However, the linearization of feedback lead to approximation of parameters which brings more rigorous convergence when some feedback parameters deviate from real values.

For such a nonholonomic under study system, the ideal control method to control the robot in kinematic level could be the one proposed by Yutaka et al [13] called Back-stepping control method. This method compares desired position and desired velocity with momentary position and momentary velocity to adjust robot's input velocity. Back-stepping method uses Lyapunov function to make sure pose error converge to zero.

Sliding mode control method is a nonlinear fast response method which is widely used in dynamic level due to its robustness to the uncertainties [14, 15]. Thanks to Switching function in sliding mode control method, the robot reaches and sticks to the sliding surface even in presence of disturbances. However, adjusting the coefficient of switching function could be challenging since the robot needs a bigger gain in reaching mode rather than sliding mode. Due to the delay between control system and physical model observed in experimental results, the big gain speed up reaching mode and consequently cause chattering problem in sliding mode [16].

Various adaptation methods has been proposed to adjust sliding mode control's gain to dealt with the chattering problem [17–21]. Rossomando et al in literature [17] proposed neural sliding mode controller in order to tune control gain in the vicinity of sliding surface to

reduce chattering in trajectory tracking. Integral sliding control method was proposed by Bessas et al [18] to solve the reaching problem in trajectory tracking by omitting the matched disturbances and minimizing the unmatched ones. Particle swarm optimization regulates the sliding surface and adjusts gain in sliding mode controller proposed by Thanok et al [20]. Exponential sliding was another method which was claimed by Mehrjerdi et al [21] to reduce chatering problem in trajectory tracking of mobile robot.

Begniniet et al proposed robust adaptive fuzzy control schema to tackle with chattering attenuation [22]. Wu et al in [23] proposed Back-stepping Fuzzy Sliding Mode in order to proportionally adjust the switching coefficient to avoid chattering problem.

In literature [22, 23], the dynamic model was derived based on the position of COM at the middle of the line connecting two diver wheels' center or the longitudinal line passing through that point. In many applications, a small change in position of COM dose not imply large trajectory tracking error and approximation in position of COM will be behaved like a noise in control system. However, when it comes to carrying off-centered heavy loads, the precision of dynamic model can affects the accuracy of trajectory tracking totally. Furthermore, for the robots which moves in narrow spaces, the accuracy of trajectory tracking gets more important because the probability of collision increases. Considering noises from sensors for calculation of robot's position and velocity will result unacceptable amount of trajectory error. Here, the necessity of having a precise dynamic model in order to minimizing the trajectory tracking error is raising.

In this study, we derived the dynamic model based on position and velocity of COM. Determination of COM's position needs force sensors to measure vertical load carried by each wheel. Wheel ground interaction forces could be determine by implementing force sensors as well which will be discussed deeply in Chapter 4. In all mentioned literature, the interaction between wheels and ground would be considered as uncertainty in dynamic model. Therefore, they literally use an open loop dynamic model completed with closed-loop kinematic model. In our understudy AMR, the amount of uncertainty in dynamic model is originated from misplacement of COM and dissipative forces of wheels. Due to the high amount of uncertainty, implementing closed-loop kinematic model is not sufficient and the necessity of closed-loop dynamic model is raising.

CHAPTER 3 KINEMATICS

3.1 Differential Drive Wheels Kinematics

An AMR with differential drive wheels consist of two laterally aligned driving wheels mounted on a central body. This mechanism is naturally unstable because the central body tends to tilt forward or backward. In order to take the advantage of this mechanism, it has to be stabilized either by implementing special control method in software level or using caster wheels in hardware level. In our case, the under study robot has caster wheels which well stabilize the mechanism. So, the kinematic model of a Differential Drive Wheel Mobile Robot (DDWMR), stabilized with caster wheel, is summarized to planar motion of the central body and does not need to stabilize the mechanism. The rotation and displacement of such a mechanism is linearly related to the angular velocity of the driving wheels. The former include the subtraction of driving wheels' angular velocities while the latter consist of the summation of them.

A typical configuration of a DDWMR is depicted in Figure 3.1. Let us attache the base frame $\mathcal{F}$ to the ground while $\mathbf{x}$, $\mathbf{y}$ and $\mathbf{z}$ are its three orthogonal unit vectors. Then, lets attache a moving frame $\mathcal{M}$ to the platform of the vehicle with its $\mathbf{y}$-axis collinear with the common revolute axis of the driving wheels and its $\mathbf{x}$-axis along the moving direction. The origin of $\mathcal{M}$ is located at the mid-point of the line connecting driving wheels' centers c_1 and c_2; where, c_1 is the center point of the right driving wheel and c_2 is the center point of the left driving wheel. The attached unit vectors $\mathbf{h}$, $\mathbf{l}$ and $\mathbf{z}$ are the x-, y- and z-axis of the moving frame $\mathcal{M}$. The radius of driving wheels is denoted by r whereas their contact points to the ground is shown by p_1 and p_2 for the right and the left driving wheels, respectively.

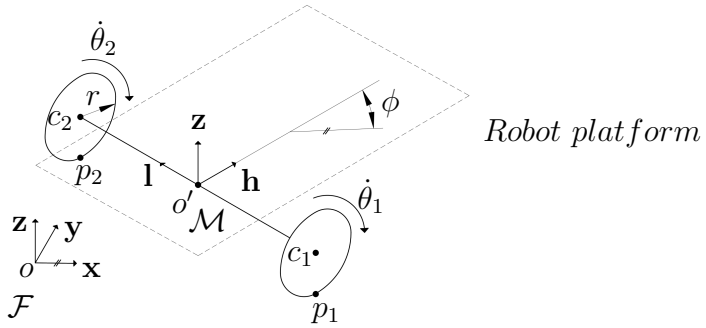

Figure 3.1 Geometry of a generic differential drive wheel mobile robot

The angular velocity of the two driving wheels known as $\dot{\theta}_1$ and $\dot{\theta}_2$ which are know as arrays of the independent velocity vector $\dot{\boldsymbol{\theta}} \equiv [\dot{\theta}_1 \ \dot{\theta}_2]^T$. The linear velocity of the DDWMR in the frame $\mathcal{M}$ is denoted by $\boldsymbol{\upsilon}$ whereas its orientation is represented by ϕ along $\mathbf{z}$. The pose vector of the DDWMR in frame $\mathcal{F}$ is presented by $\mathbf{q} \equiv [x \ y \ \phi]^T$. In order to derive the kinematic model of the DDWMR, we need to link the independent velocity vector $\dot{\boldsymbol{\theta}}$ in frame $\mathcal{M}$ to the twist vector $\dot{\mathbf{q}} \equiv [\dot{x} \ \dot{y} \ \dot{\phi}]^T$ in frame $\mathcal{F}$ whereas $\dot{\mathbf{q}}$ is nothing but the time derivative of robot pose $\mathbf{q}$.

Lets define the position of the driving wheels' centers c_1 and c_2 in frame $\mathcal{F}$ as vector $\vec{oc}_i$ for $i = 1, 2$ by:

$$\vec{oc}_i = \vec{op}_i + \vec{p_ic}_i = \vec{op}_i + r\mathbf{z} \tag{3.1}$$

Considering the angular velocity of the left and right driving wheels as $\boldsymbol{\omega}_i = [0 \ \dot{\theta}_i \ \dot{\phi}]^T$ in frame $\mathcal{M}$ and after taking the time derivative of eq.(3.1) we have:

$$\dot{\vec{oc}}_i = \dot{\vec{op}}_i + r\dot{\theta}_i\mathbf{h} \tag{3.2}$$

where $\dot{\vec{op}}_i$ is the velocity of the driving wheels' contact point to the ground $\vec{op}_i$. Under the assumption of pure rolling, $\dot{\vec{op}}_i$ is zero in frame $\mathcal{M}$. Let's define δ_i as the slippage angle which is the displacement loss because of slipping of a driving wheel and ϵ as skidding distance which is the lateral displacement of the robot [24]. Therefore, the velocity of driving wheel's center in eq.(3.2) will be as follow:

$$\dot{\vec{oc}}_i = (r\dot{\theta}_i - \dot{\delta}_i)\mathbf{h} - \dot{\epsilon}\mathbf{l} \tag{3.3}$$

Now, in order to calculate the velocity of point o' in fram $\mathcal{M}$, its position needs to be defined first as:

$$\vec{oo'} = \vec{oc}_i + \vec{c}_io' \tag{3.4}$$

where :

$$\vec{c_1o'} = -d/2\mathbf{h}, \quad \vec{c_2o'} = d/2\mathbf{h} \tag{3.5}$$

Knowing the angular velocity of the DDWMR's base as $\dot{\phi}\mathbf{z}$ and taking the time derivative of eq.(3.4) yields:

$$\dot{\vec{oo'}}_1 = (r\dot{\theta}_1 - \dot{\delta}_1 - \frac{d}{2})\mathbf{h} - \dot{\epsilon}\mathbf{l}, \quad \dot{\vec{oo'}}_2 = (r\dot{\theta}_1 - \dot{\delta}_1 + \frac{d}{2})\mathbf{h} - \dot{\epsilon}\mathbf{l} \tag{3.6}$$

Then, by solving eq.(3.6), the linear and angular velocity of a DDWMR in frame $\mathcal{M}$ will be as follow:

$$\dot{\boldsymbol{\phi}} = (\frac{r}{d}(\dot{\theta}_1 - \dot{\theta}_2) - \frac{1}{d}(\dot{\delta}_1 - \dot{\delta}_2))\mathbf{z} \tag{3.7}$$

$$\boldsymbol{\upsilon} = (\frac{r}{2}(\dot{\theta}_1 + \dot{\theta}_2) - \frac{1}{2}(\dot{\delta}_1 + \dot{\delta}_2))\mathbf{h} - \dot{\epsilon}\mathbf{l} \tag{3.8}$$

Since, in our study the AMR does not demand to cope with the high speed maneuver, the assumption of pure rolling is applicable. Therefore, further in this study, we consider $\dot{\delta}_i$ and $\dot{\epsilon}$ as zero. Now, using eq.(3.7) and eq.(3.8), the twist of the DDWMR in frame $\mathcal{M}$ is defined by $\mathbf{v} \equiv [\boldsymbol{\upsilon}\ \dot{\phi}]$ considering independent velocity vector $\dot{\boldsymbol{\theta}}$ as:

$$\mathbf{v} = \mathbf{K}\dot{\boldsymbol{\theta}}, \quad \mathbf{K} = \begin{bmatrix} \frac{r}{2} & \frac{r}{2} \\ 0 & 0 \\ \frac{r}{d} & -\frac{r}{d} \end{bmatrix} \tag{3.9}$$

To translate the motion from moving coordinate system $\mathcal{M}$ to fixed coordinate system $\mathcal{F}$, the rotation matrix along $\mathbf{z}$ is used. As a result, the twist vector $\dot{\boldsymbol{q}}$ in frame $\mathcal{F}$, will be related to the twist vector $\mathbf{v}$ in frame $\mathcal{M}$ as follow:

$$\dot{\mathbf{q}} = \mathbf{R}(\phi)\mathbf{v}, \quad \mathbf{R}(\phi) = \begin{bmatrix} \cos\phi & -\sin\phi & 0 \\ \sin\phi & \cos\phi & 0 \\ 0 & 0 & 1 \end{bmatrix} \tag{3.10}$$

So, the Jacobian matrix which links the twist vector $\dot{\mathbf{q}}$ to the independent velocity vector $\dot{\boldsymbol{\theta}}$ is:

$$\dot{\mathbf{q}} = \mathbf{J}\dot{\boldsymbol{\theta}} \quad , \mathbf{J} \equiv \mathbf{R}(\phi)\mathbf{K} = \begin{bmatrix} \cos\phi & -\sin\phi & 0 \\ \sin\phi & \cos\phi & 0 \\ 0 & 0 & 1 \end{bmatrix} \begin{bmatrix} \frac{r}{2} & \frac{r}{2} \\ 0 & 0 \\ \frac{r}{d} & -\frac{r}{d} \end{bmatrix} \tag{3.11}$$

The eq.(3.11) will be used in chapter 5 to deal with path tracking problem.

3.2 Kinematics of AMR

In section 3.1, the kinematic model of a DDWMR has been derived considering the velocity of point o' which is at the middle of the line connecting driving wheels' centers. In many cases, such a mechanism has been used considering the point o' as the COM. However, as explained in Chapter 1, the COM of the under study robot is variable due to loading and unloading weight on the robot's platform. In order to derive the dynamic model of the AMR around its COM, the velocity and location of its COM matters. So, we need to obtain the velocity of new COM knowing its location. Let us assume the loaded weight on the AMR relocate the location of COM from point o' to the point c which called Instantaneous Center Of Mass (ICOM). The location of c in moving frame $\mathcal{M}$ is presented by b and a along $\mathbf{h}$ and

l respectively shown in Figure 3.2.

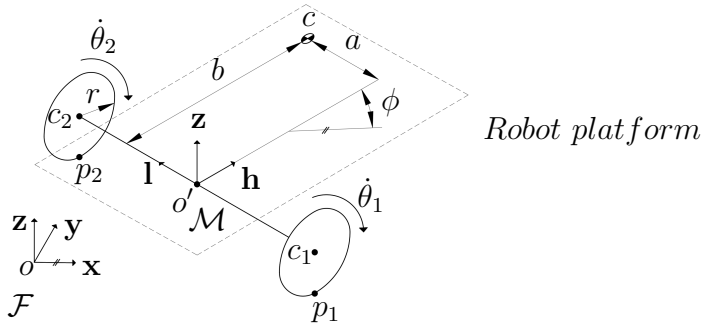

Figure 3.2 Geometry of an AMR with variable COM

The equation 3.4 could be rewritten considering point c as ICOM as follow:

$$\vec{oc} = \vec{oc}_i + \vec{c_ic} \tag{3.12}$$

where :

$$\vec{c_1c} = b\mathbf{h} + (\frac{d}{2} + a)\mathbf{l}, \quad \vec{c_2c} = b\mathbf{h} - (\frac{d}{2} - a)\mathbf{l} \tag{3.13}$$

Knowing the angular velocity of the robot's base as $\dot{\phi}\mathbf{k}$ and taking the time derivative of eq.(3.12) yields:

$$\dot{\vec{oc}} = (r\dot{\theta}_i - \dot{\delta}_i \mp \frac{d}{2} - a)\mathbf{h} - (\dot{\epsilon} + b\dot{\phi})\mathbf{l} \tag{3.14}$$

By solving eq.(3.14) for $i = 1, 2$, the angular velocity of the AMR around its ICOM in frame $\mathcal{M}$ will be the same as eq.(3.7) for a DDWMR but, the linear velocity of ICOM, $\boldsymbol{\upsilon}_c$, will be as follow:

$$\boldsymbol{\upsilon}_c = \begin{bmatrix} \frac{r}{2}(\dot{\theta}_1 + \dot{\theta}_2) - \frac{1}{2}(\dot{\delta}_1 + \dot{\delta}_2) - \frac{ar}{d}(\dot{\theta}_1 - \dot{\theta}_2) + \frac{a}{d}(\dot{\delta}_1 - \dot{\delta}_2) \\ \frac{br}{2}(\dot{\theta}_1 - \dot{\theta}_2) - \frac{b}{d}(\dot{\delta}_1 - \dot{\delta}_2) - \dot{\epsilon} \\ 0 \end{bmatrix} \tag{3.15}$$

As mentioned in the Section 3.1, the assumption of pure rolling is applicable due to relatively slow maneuver of AMR; so, we can ignore the slippage and skid of the driving wheels. Thus, the angular velocity of AMR around its ICOM would be like a DDWMR as eq.(3.8) and ICOM's linear velocity will be simplified as:

$$\boldsymbol{\upsilon}_c = [\frac{r}{2}(\dot{\theta}_1 + \dot{\theta}_2) - \frac{ar}{d}(\dot{\theta}_1 - \dot{\theta}_2)]\mathbf{h} + [(\frac{br}{d}(\dot{\theta}_1 - \dot{\theta}_2)]\mathbf{l} \tag{3.16}$$

The twist of an AMR along its ICOM, $\mathbf{v}_c \equiv [\boldsymbol{v}_c \ \dot{\phi}]$ in frame $\mathcal{M}$ can be shown as:

$$\mathbf{v}_c = \mathbf{K}_c \begin{bmatrix} \dot{\theta}_1 \\ \dot{\theta}_2 \end{bmatrix}, \quad \mathbf{K}_c = \begin{bmatrix} \frac{r}{2} - \frac{ar}{d} & \frac{r}{2} + \frac{ar}{d} \\ \frac{br}{d} & -\frac{br}{d} \\ \frac{r}{d} & -\frac{r}{d} \end{bmatrix} \tag{3.17}$$

In addition, the twist vector of an AMR in frame $\mathcal{F}$, $\dot{\mathbf{q}}_c$, is obtained using rotational matrix $\mathbf{R}(\phi)$ as:

$$\dot{\mathbf{q}}_c = \mathbf{R}(\phi)\mathbf{v} \tag{3.18}$$

where $\mathbf{R}(\phi)$ has been introduced in eq.(3.10). So, the Jacobian matrix which links the twist vector of AMR in frame $\mathcal{F}$ along its ICOM, to the AMR's independent velocity vector $\dot{\boldsymbol{\theta}}$ is defined as:

$$\mathbf{J}_c = \begin{bmatrix} \cos\phi & -\sin\phi & 0 \\ \sin\phi & \cos\phi & 0 \\ 0 & 0 & 1 \end{bmatrix} \begin{bmatrix} \frac{r}{2} - \frac{ar}{d} & \frac{r}{2} + \frac{ar}{d} \\ \frac{br}{d} & -\frac{br}{d} \\ \frac{r}{d} & -\frac{r}{d} \end{bmatrix} \tag{3.19}$$

The eq.(3.19) is used in Chapter.5 to solve dynamic model.

3.3 Caster Wheel Kinematics

Caster wheels in DDWMR stabilize the system and passively follow the dictated path by driving wheels. Caster wheel, as shown in Figure 3.3, is a single wheel with two axis, one horizontally in wheel's center for rolling and one vertically off the wheel's center for turning. The off center distance of caster's pivot point is illustrated by e whereas its rotation shown by θ_c. When the driving wheels are rolling and the orientation of the caster wheel is not along the orientation of the platform, the contact point of the caster wheel to the ground generates a torque along the vertical axis. This generated torque gradually rotates the caster wheel to the dictated orientation by the platform. This stage called transition mode and after that caster wheel's orientation remains fixed as long as the platform keeps turning with fixed turning radius shown by s in Figure A.3. This fixed angle which is proportional to the turning radius is called final angle. Under the assumption of *no slipping* and *no skidding*, the kinematic model of a DDWMR, shown in eq.(3.9), does not express the orientation of the caster wheels. The steering angle of a caster wheel which have been studied in [2] is nothing but the angle between the velocity of the caster wheel's pivot point, Figure 3.3, and **h**-axis of the frame $\mathcal{M}$. Moreover, the proposed method in literature [2] is not able to consider the transition mode which is the caster orientation before reaching the final angle. Hence, we propose a mathematical model which computes the rotation angle of a caster wheel along its

vertical axis in transition mode.

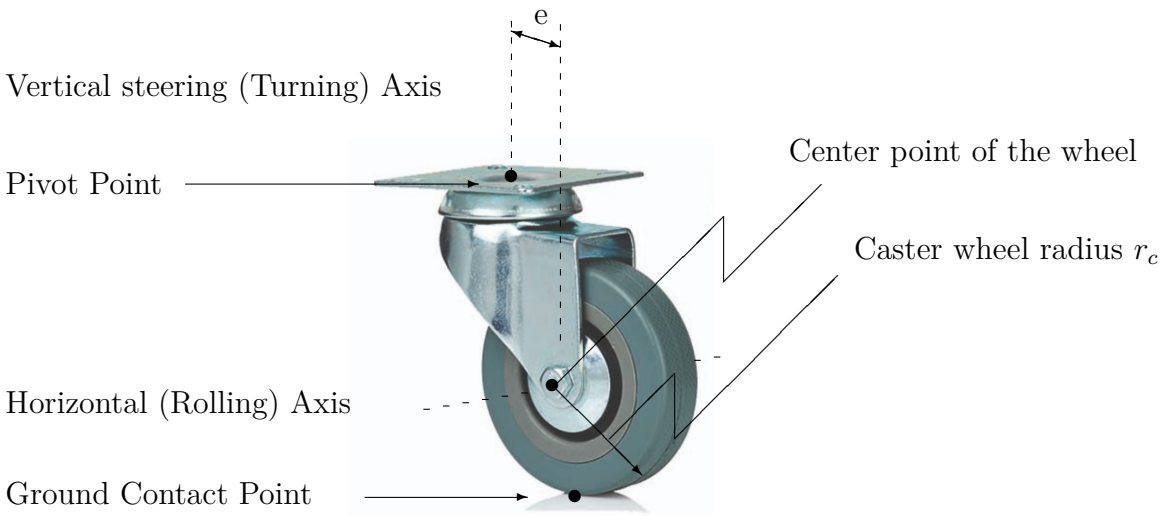

Figure 3.3 A typical caster wheel

Let us consider Figure A.3 which shows a differential drive mechanism mounted on a platform with four casters spread at four corners while the vehicle is turning left and rotates around its Instantaneous Center Of Rotation (ICOR) denoted by point c_r. The distance between the point c_r to the origin of the frame $\mathcal{M}$ is called turning radius and shown by s. During any rotation, the ICOR remains along the **l**-axis of the frame $\mathcal{M}$. The distance between the pivot point of each caster wheel n_i, and ICOR point c_r, is shown by l_i for $i = 1$ to 4. The angle between the orientation of each caster wheel and the **h**-axis of frame $\mathcal{M}$ is expressed by ψ_i for $i = 1$ to 4. The angle made by the line connecting the caster wheels' pivot point and ICOR point with **h**-axis of frame $\mathcal{M}$ is denoted by α_i for $i = 1$ to 4. In this thesis, the position in which the angle ψ_i is zero called caster's neutral position.

In this Section we study two different scenarios of caster wheels as follow:

- The situation where the casters are in neutral position and the robot starts turning.
- The casters have an angle and the robot moves straight so the casters return to their neutral position.

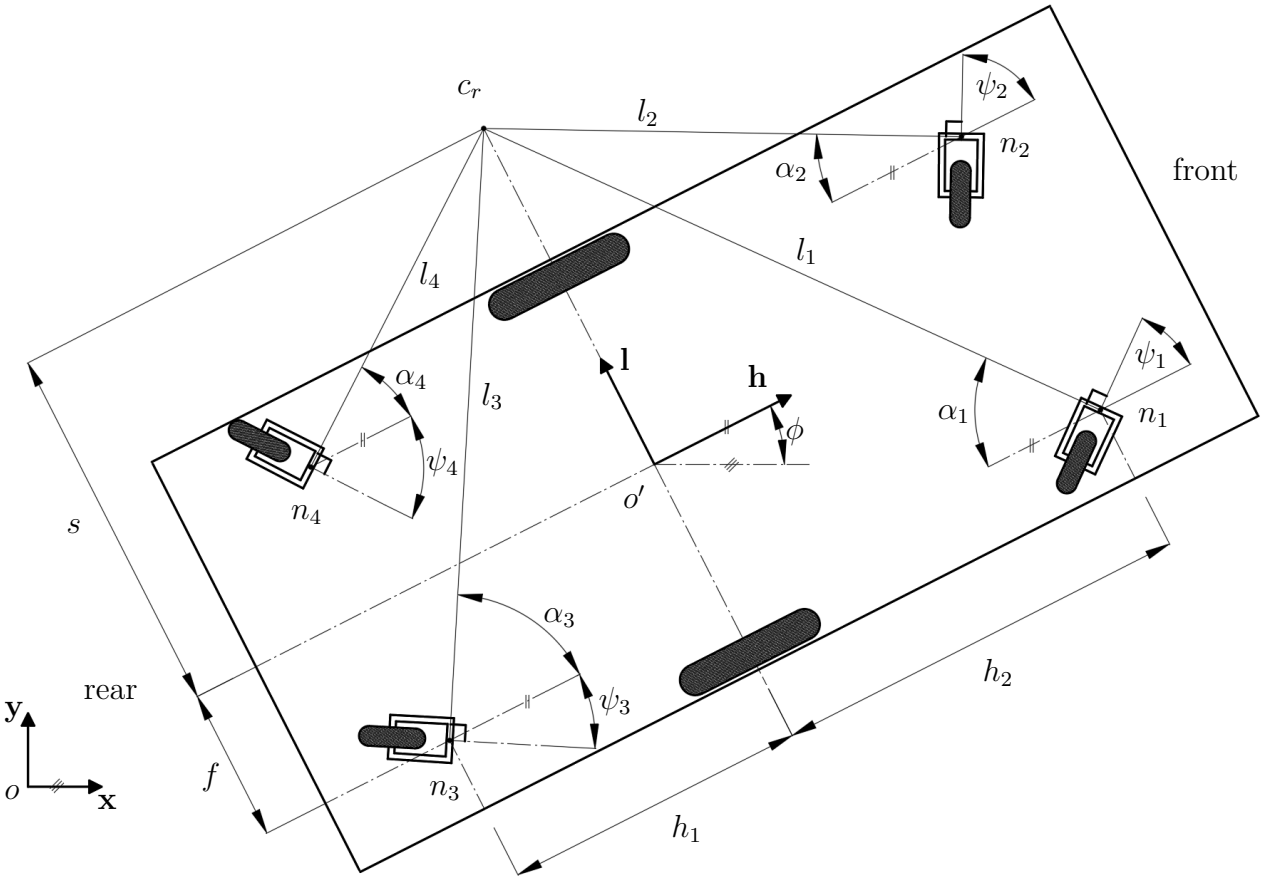

Figure 3.4 Caster wheels orientations relative to the ICOR

3.3.1 Turning on neutral position

In this section, we consider the change in the orientation of caster wheels start from neutral position what we called transition mode. Considering Figure A.3, when the platform starts turning around a vertical axis passing through ICOR, the velocity of the pivot point of i^{th} caster with respect to the point c_r in the frame $\mathcal{F}$, is the result of pure rotation such that:

$$\mathbf{v}_{n_i} = l_i \dot{\phi} \begin{bmatrix} \sin(\alpha_i - \phi) \\ \cos(\alpha_i - \phi) \end{bmatrix} \tag{3.20}$$

On the other hand, the velocity of each caster wheel pivot point could be decomposed into two perpendicular velocities. First, $r_c \dot{\theta}_c^i$ which is the result of rolling motion of the i^{th} caster wheel. Second, $e\dot{\phi}_i$ which is consequence of rotation of the i^{th} caster wheel around its contact

point to the ground. Expressing these two velocities in the frame $\mathcal{F}$, yields:

$$\mathbf{v}_{n_i} = \begin{bmatrix} r_c\dot{\theta}_c^i \cos\psi_i - e\dot{\psi}_i \sin\psi_i \\ r_c\dot{\theta}_c^i \sin\psi_i + e\dot{\psi}_i \cos\psi_i \end{bmatrix} \tag{3.21}$$

Once comparing eqs. (A.9) and (A.10), we get:

$$\tan\psi_i = \frac{l_i\dot{\phi}\cos(\alpha_i - \phi) - e\dot{\psi}_i \cos\psi_i}{l_i \sin(\alpha_i - \phi) + e\dot{\psi}_i \sin\psi_i} \tag{3.22}$$

When the robot starts turning, ψ_i will rise and by keep turning of the robot, the ψ_i reaches to its final orientation $[\psi_i]_f$ and $\dot{\psi}_i$ gets zero. Applying this condition to the eq.(3.22) yields:

$$[\psi_i]_f = \frac{\pi}{2} + \phi - \alpha_i, \tag{3.23}$$

The angle between the line connecting the pivot point of each caster wheel and ICOR point with respect to the **h**-axis will be as follow:

$$\alpha_1 = \tan^{-1}(\frac{s+f}{h_2}), \quad \alpha_2 = \tan^{-1}(\frac{s-f}{h_2}), \tag{3.24}$$

$$\alpha_3 = \tan^{-1}(\frac{s+f}{h_1}), \quad \alpha_4 = \tan^{-1}(\frac{s-f}{h_1}), \tag{3.25}$$

The lateral displacement of each caster's pivot point in the fixed frame $\mathcal{F}$ can be considered from two point of views. Firstly, the lateral displacement of a point n_i is due to the rotation around ICOR. Secondly, this lateral displacement is because of the rotation of caster wheel around its contact point to the ground. In order to meet the assumption of pure rolling, these two lateral displacement must be equal which yields the following kinematic constrain:

$$\sin\psi_i - \sin[\psi_i]_{init} = \frac{||l_i||}{e}\ (\sin(\alpha_i - \phi) - \sin\alpha_i) \tag{3.26}$$

where $[\psi_i]_{init}$ is the initial value of ψ_i which considered zero because the motion has started from neutral position of caster wheels.

3.3.2 Turning to neutral position

When the vehicle start going straight forward after turning, the heading velocity of the robot will be $r\dot{\theta}$, where $\dot{\theta}$ is the angular velocity of the driving wheels. Moreover, by moving robot forward, caster wheels which are not yet in neutral orientation, will do so with a kinematic relationship. As shown in Figure A.3, each caster wheel pivot n_i must follow the vehicle,

whereas in the frame $\mathcal{M}$, the heading velocity of the i^{th} wheel pivot point is given by $r_c\dot{\theta_c}^{i}$ and the velocity of the caster wheel caused by rotation around the contact point to the ground is $e\dot{\psi}_i$. Since the sum of these two vectors must results in the velocity of the robot, we have:

$$\text{Along } \mathbf{h} \quad : \quad r\dot{\theta} = r_c\dot{\theta}_c^i \cos\psi_i + e\dot{\psi}_i \sin\psi_i \tag{3.27}$$

$$\text{Along } \mathbf{l} \quad : \quad e\dot{\psi}_i \cos\psi_i = r_c\dot{\theta}_c^i \sin\psi_i \tag{3.28}$$

Upon substitution of eq.(A.16) into (A.15) in order to get ride of $\dot{\theta}_c^i$, we obtain:

$$\frac{r\dot{\theta}}{e} = \frac{\dot{\psi}_i}{\sin\psi_i} \tag{3.29}$$

The integral of eq.(A.17) with respect to the time between the initial condition, $[\psi_i]_f$ from previous stage, and the final condition, ψ_i, can be calculated as:

$$\int \frac{r\dot{\theta}}{e} = \int_{[\psi_i]_f}^{\psi_i} \frac{\dot{\psi}_i}{\sin\psi_i} \tag{3.30}$$

$$\frac{r\theta}{e} = \ln[\tan([\psi_i]_f/2)] - \ln[\tan(\psi_i/2)] \tag{3.31}$$

3.3.3 Simulation Results

The mathematical model of eqs.(A.12, 3.26, A.19), for determining the caster wheel orientation ψ_i, is compared with the dynamic simulation of the Webot platform [9] along two different scenarios. This multi-platform desktop application is open source and used to simulate robots. Dimensions used in simulations are shown in Table A.1. In scenario 1, the platform moves straight forward to make sure all the caster wheels are along robot platform and then turns with two different radii. We select for an easy interpretation such as a) having an ICOR at point o' so that the robot is turning around itself $(s = 0)(mm)$; b) having ICOR at one driving wheel contact point to the ground so that the platform turns around one of its driving wheels $(s = 344)(mm)$. In scenario 2, the platform starts going straight forward after turning with two different radius c) from $(s = 0)(mm)$; and d) from $(s = 344)(mm)$.

Table 3.1 Geometrical dimensions of the AGV used in simulation (mm)

h_1	h_2	s	e	r_c	r
631	562	250	34	38	100

Apparently from Figure A.4, the mathematical model is a rather coarse in scenarios 1 and 2. One possible reason for fluctuation of simulation value in scenario 1, could be, the effect of centrifugal force on the caster wheels. It means, the centrifugal forces try to turn caster wheels more by push them to skid. But, in scenario 2, the robot goes straight and the centrifugal forces does not affect caster wheels much. In scenario 2, the gaps between the simulation and mathematical model are less in bigger turning radius. It seems, caster wheels tend to skid more because they must turn more at shorter amount of time. Moreover, we do not have much information about the elements included into the dynamic model of Webots [9].

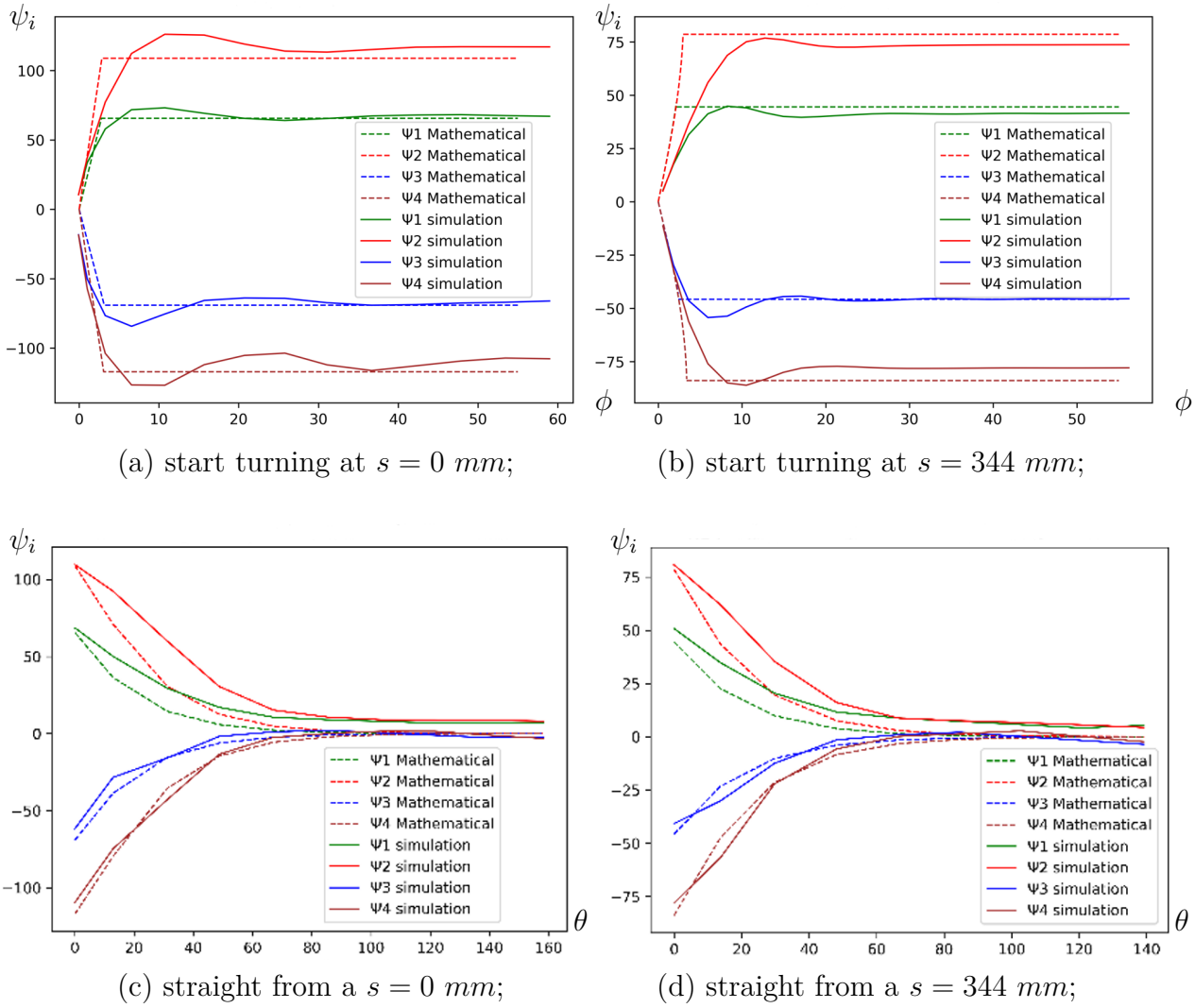

(a) start turning at $s = 0\ mm$; (b) start turning at $s = 344\ mm$;

(c) straight from a $s = 0\ mm$; (d) straight from a $s = 344\ mm$;

Figure 3.5 Mathematical model and Webot's dynamic simulation of caster wheel orientation: scenario 1, turning from neutral position of caster wheels a) turning with $(s = 0)\ (mm)$; b) turning with $(s = 344)\ (mm)$; scenario 2, going straight forward after turning c) from a turning of $(s = 0)\ (mm)$; and d) from turning of $(s = 344)\ (mm)$.

CHAPTER 4 DYNAMICS

4.1 AMR's Dynamic Model

The dynamic model is the link between the pure trajectory tracking and the actual trajectory tracking. Caster wheels in an AMR, shown in Figure 3.3, are one of the main sources of uncertainty in dynamic models. A wheel faces three types of dissipative forces namely rolling resistance, turning friction and skidding friction and all of them are a function of wheel's normal load [26]. Under the assumption of unwell distributed load on the AMR, normal load and resistance force of each caster wheel applied to the robot's platform varies. This unbalance, leads to an unwilling disturbance torque and consequently error in the robot's orientation. As a result, the interaction force between wheels and ground can not be neglected in a dynamic model of an AMR with variable COM. Moreover, the off center location of mass changes COM totally. Therefore, the dynamic models based on a fixed COM will not be faultless. To tackle with this problem, the employment of 3D force sensors is proposed to measure the horizontal dissipative force and vertical load of each wheel. Dissipative forces can be directly measured by force sensors installed on the robot's platform and sensed vertical loads helps to find COM location. Let's divide an AMR to three bodies, namely right driving wheel as the first body, left driving wheel as the second body and the rest, including carrying weight and excluding caster wheels, considered as the platform and third boy as shown in Figure 4.1.

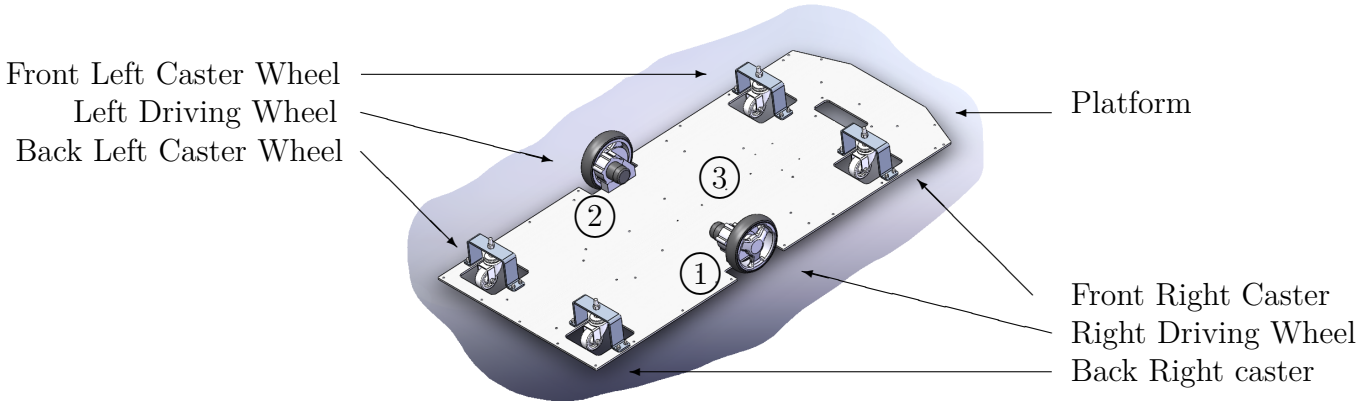

Figure 4.1 A typical configuration of an AMR and numbers associated to each body

The twist $\mathbf{t}_i \equiv [\dot{\mathbf{c}}_i \ \boldsymbol{\omega}_i]^T$ of each body which consist of the linear and angular velocities of the associated body's COM will be defined as follow:

$$\mathbf{t}_i = \mathbf{T}_i\dot{\boldsymbol{\theta}}, \quad \mathbf{T}_1 = \overset{\text{Right Wheel}}{\begin{bmatrix} 0 & 0 \\ 1 & 0 \\ \frac{r}{d} & -\frac{r}{d} \\ r & 0 \\ 0 & 0 \\ 0 & 0 \end{bmatrix}}, \quad \mathbf{T}_2 = \overset{\text{Left Wheel}}{\begin{bmatrix} 0 & 0 \\ 0 & 1 \\ \frac{r}{d} & -\frac{r}{d} \\ 0 & r \\ 0 & 0 \\ 0 & 0 \end{bmatrix}}, \quad \mathbf{T}_3 = \overset{\text{Platform and Load}}{\begin{bmatrix} 0 & 0 \\ 0 & 0 \\ \frac{r}{d} & -\frac{r}{d} \\ \frac{r}{2} - \frac{ar}{d} & \frac{r}{2} + \frac{ar}{d} \\ \frac{br}{d} & -\frac{br}{d} \\ 0 & 0 \end{bmatrix}} \tag{4.1}$$

where $\mathbf{T} \equiv [\mathbf{T}_1 \ \mathbf{T}_2 \ \mathbf{T}_3]^T$ is a 18×2 twist shaping matrix of the robot which links the robot's twist $\mathbf{t} \equiv [\mathbf{t}_1 \ \mathbf{t}_2 \ \mathbf{t}_3]^T$ to the vector of independent velocity $\dot{\boldsymbol{\theta}} = [\dot{\theta}_1 \ \dot{\theta}_2]^T$. The frame $\mathcal{M}$ has planar motion and only one rotation which is $\boldsymbol{\phi} \equiv [0 \ 0 \ \phi]^T$. Considering the rotation of the platform, the derivative of $\mathbf{h}$ and $\mathbf{l}$ unit vectors would be as follow:

$$\dot{\mathbf{h}} = \dot{\phi}\mathbf{k} \times \mathbf{h} = \dot{\phi}\mathbf{l}, \qquad \dot{\mathbf{l}} = \dot{\phi}\mathbf{k} \times \mathbf{l} = -\dot{\phi}\mathbf{h} \tag{4.2}$$

Considering the rotation of wheels, the derivative of $\mathbf{h}$ and $\mathbf{l}$ unit vectors would be as follow:

$$\dot{\mathbf{h}} = (\dot{\phi}\mathbf{k} + \dot{\theta}_i\mathbf{l}) \times \mathbf{h} = \dot{\phi}\mathbf{l} - \dot{\theta}_i\mathbf{k}, \quad \dot{\mathbf{l}} = (\dot{\phi}\mathbf{k} + \dot{\theta}_i\mathbf{l}) \times \mathbf{l} = -\dot{\phi}\mathbf{h}, \quad \dot{\mathbf{k}} = (\dot{\phi}\mathbf{k} + \dot{\theta}_i\mathbf{l}) \times \mathbf{k} = \dot{\theta}_i\mathbf{h} \tag{4.3}$$

Using equation (4.2,4.3), the time-derivative of twist shaping matrix $\dot{\mathbf{T}} \equiv [\dot{\mathbf{T}}_1 \ \dot{\mathbf{T}}_2 \ \dot{\mathbf{T}}_3]^T$ is going to be a 18×2 matrix with following sub matrices:

$$\dot{\mathbf{T}}_1 = \begin{bmatrix} \frac{r}{d}\dot{\theta}_2 & -\frac{r}{d}\dot{\theta}_1 \\ 0 & 0 \\ 0 & 0 \\ 0 & 0 \\ \frac{r^2}{d}(\dot{\theta}_1 - \dot{\theta}_2) & 0 \\ r\dot{\theta}_1 & 0 \end{bmatrix}, \quad \dot{\mathbf{T}}_2 = \begin{bmatrix} \frac{r}{d}\dot{\theta}_2 & -\frac{r}{d}\dot{\theta}_1 \\ 0 & 0 \\ 0 & 0 \\ 0 & 0 \\ 0 & \frac{r^2}{d}(\dot{\theta}_1 - \dot{\theta}_2) \\ 0 & r\dot{\theta}_2 \end{bmatrix}$$

$$\dot{\mathbf{T}}_3 = \begin{bmatrix} 0 & 0 \\ 0 & 0 \\ 0 & 0 \\ -b(\frac{r}{d})^2(\dot{\theta}_1 - \dot{\theta}_2) & b(\frac{r}{d})^2(\dot{\theta}_1 - \dot{\theta}_2) \\ (\frac{r}{d})^2(\frac{d}{2} - a)(\dot{\theta}_1 - \dot{\theta}_2) & (\frac{r}{d})^2(\frac{d}{2} + a)(\dot{\theta}_1 - \dot{\theta}_2) \\ 0 & 0 \end{bmatrix} \tag{4.4}$$

Furthermore, the 18×18 mass matrix of the whole system $\mathbf{M}$, which contains the 6×6 mass matrix of each body $\mathbf{M}_i$ and 3×3 inertia matrix of each body $\mathbf{I}_i$ are given as follow:

$$\mathbf{M} \equiv \begin{bmatrix} \mathbf{M}_1 & \mathbf{0} & \mathbf{0} \\ \mathbf{0} & \mathbf{M}_2 & \mathbf{0} \\ \mathbf{0} & \mathbf{0} & \mathbf{M}_3 \end{bmatrix}, \quad \mathbf{M}_i \equiv \begin{bmatrix} \mathbf{I}_i & \mathbf{0} \\ \mathbf{0} & m_i\mathbf{1} \end{bmatrix}, \quad \mathbf{I}_i \equiv \begin{bmatrix} I_{hi} & 0 & 0 \\ 0 & I_{li} & 0 \\ 0 & 0 & I_{zi} \end{bmatrix} \tag{4.5}$$

where $\mathbf{0}$ and $\mathbf{1}$ are 3×3 zero and identity matrices, respectively. In eq.(4.5), m_i is the mass of i^{th} body and I_{hi}, I_{li} and I_{zi} are the moment of inertia of i^{th} body relative to its COM along $\mathbf{h}$,$\mathbf{l}$ and $\mathbf{z}$ axes, respectively, for $i = 1, 2$ *and* 3. The moment of inertia and the mass of robot's platform, are calculated using the vertical loads applied to the platform by wheels measured by force sensors. The angular velocity matrix of i^{th} body $\mathbf{W}_i$ which is a sub matrix of 18×18 angular velocity matrix $\mathbf{W}$ can be defined as follow:

$$\mathbf{W} \equiv \begin{bmatrix} \mathbf{W}_1 & \mathbf{0}_{6\times6} & \mathbf{0}_{6\times6} \\ \mathbf{0}_{6\times6} & \mathbf{W}_2 & \mathbf{0}_{6\times6} \\ \mathbf{0}_{6\times6} & \mathbf{0}_{6\times6} & \mathbf{W}_3 \end{bmatrix}, \quad \mathbf{W}_i \equiv \begin{bmatrix} \mathbf{\Omega}_i & \mathbf{0}_{3\times3} \\ \mathbf{0}_{3\times3} & \mathbf{0}_{3\times3} \end{bmatrix} \tag{4.6}$$

where $\mathbf{0}_{6\times6}$ is a 6×6 zero matrix and $\mathbf{\Omega}_i$ is the cross product matrix of the angular velocity vector of each body as follow:

$$\begin{aligned} \mathbf{\Omega}_1 &\equiv \begin{bmatrix} 0 & -\frac{r}{d}(\dot{\theta}_1 - \dot{\theta}_2) & \dot{\theta}_1 \\ \frac{r}{d}(\dot{\theta}_1 - \dot{\theta}_2) & 0 & 0 \\ -\dot{\theta}_1 & 0 & 0 \end{bmatrix}, \quad \mathbf{\Omega}_2 \equiv \begin{bmatrix} 0 & -\frac{r}{d}(\dot{\theta}_1 - \dot{\theta}_2) & \dot{\theta}_2 \\ \frac{r}{d}(\dot{\theta}_1 - \dot{\theta}_2) & 0 & 0 \\ -\dot{\theta}_2 & 0 & 0 \end{bmatrix} \\ \mathbf{\Omega}_3 &\equiv \begin{bmatrix} 0 & -\frac{r}{d}(\dot{\theta}_1 - \dot{\theta}_2) & \dot{\theta}_1 \\ \frac{r}{d}(\dot{\theta}_1 - \dot{\theta}_2) & 0 & 0 \\ 0 & 0 & 0 \end{bmatrix} \end{aligned} \tag{4.7}$$

Now, using natural orthogonal complementary method [27], the dynamic model of an AMR with variable COM can be derived as:

$$\mathbf{I}(\theta)\ddot{\boldsymbol{\theta}} = \mathbf{C}(\theta, \dot{\theta})\dot{\boldsymbol{\theta}} + \mathbf{\Upsilon} + \boldsymbol{\gamma} + \boldsymbol{\delta} \tag{4.8}$$

or alternatively:

$$\mathbf{T}^T\mathbf{M}\mathbf{T}\ddot{\boldsymbol{\theta}} = -\mathbf{T}^T(\mathbf{M}\dot{\mathbf{T}} + \mathbf{W}\mathbf{M}\mathbf{T})\dot{\boldsymbol{\theta}} + \mathbf{T}^T(\mathbf{w}^{\mathbf{A}} + \mathbf{w}^{\mathbf{G}} + \mathbf{w}^{\mathbf{D}}) \tag{4.9}$$

where:

$\mathbf{I} \equiv \mathbf{T}^T\mathbf{M}\mathbf{T}$ Matrix of generalized inertia

$\mathbf{C} \equiv -\mathbf{T}^T(\mathbf{M}\dot{\mathbf{T}} + \mathbf{W}\mathbf{M}\mathbf{T})$ Matrix of convective inertia

$\boldsymbol{\tau} \equiv \mathbf{T}^T\mathbf{w}^A$ Vector of driving force

$\boldsymbol{\gamma} \equiv \mathbf{T}^T\mathbf{w}^G$ Vector of gravity force

$\boldsymbol{\Upsilon} \equiv \mathbf{T}^T\mathbf{w}^D$ Vector of dissipative force.

Since the robot has planar motion, the gravity wrench has been ignored. The acting wrench of the robot is 16×1 column including the acting wrench of each body as follow:

$$\mathbf{w}^A = \begin{bmatrix} \mathbf{w}_1^A \\ \mathbf{w}_2^A \\ \mathbf{w}_3^A \end{bmatrix}, \quad \mathbf{w}_1^A = \overset{\text{Right wheel}}{\begin{bmatrix} 0 \\ \tau_1 \\ 0 \\ 0 \\ 0 \\ 0 \end{bmatrix}}, \quad \mathbf{w}_2^A = \overset{\text{Left wheel}}{\begin{bmatrix} 0 \\ \tau_2 \\ 0 \\ 0 \\ 0 \\ 0 \end{bmatrix}}, \quad \mathbf{w}_3^A = \overset{\text{Platform}}{\begin{bmatrix} 0 \\ 0 \\ 0 \\ 0 \\ 0 \\ 0 \end{bmatrix}} \tag{4.10}$$

where τ_1 and τ_2 are the generated torque of the driving wheels' motors. The arrays of the dissipative wrench are filled by the values read from force sensors as follow:

$$\mathbf{w}^D = \begin{bmatrix} \mathbf{w}_1^D \\ \mathbf{w}_2^D \\ \mathbf{w}_3^D \end{bmatrix}, \quad \mathbf{w}_1^D = \overset{\text{Right wheel}}{\begin{bmatrix} 0 \\ -rf_{h1} \\ 0 \\ 0 \\ 0 \\ 0 \end{bmatrix}}, \quad \mathbf{w}_2^D = \overset{\text{Left wheel}}{\begin{bmatrix} 0 \\ -rf_{h2} \\ 0 \\ 0 \\ 0 \\ 0 \end{bmatrix}}, \quad \mathbf{w}_3^A = \overset{\text{Platform}}{\begin{bmatrix} 0 \\ 0 \\ \mathbf{m}_c \\ \sum_{n=1}^{j} f_{hj} \\ \sum_{n=1}^{j} f_{lj} \\ 0 \end{bmatrix}} \tag{4.11}$$

The f_{h_j} and f_{l_j} stand for longitudinal and lateral forces sensed with j^{th} force sensor. The number of each force sensor associated to the each wheel shown in Figure 4.1, is listed in

Table.(4.1) as follow:

Table 4.1 Number assigned to the force sensor of each wheel

Wheel Name	Force sensor Number (j)
Right driving wheel	1
Left driving wheel	2
Front right caster	3
Front left caster	4
Rear right caster	5
Rear left caster	6

The $\mathbf{m}_c$, used in eq.(4.11), is the summation of torques, caused by horizontal dissipative forces of caster wheels, along the vertical line passing through the COM as:

$$\mathbf{m}_c \equiv (f_{h3} + f_{h5})(f + a) + (f_{l3} + f_{l4})(h_2 - b) - (f_{h4} + f_{h6})(f - a) - (f_{l5} + f_{l6})(h_1 + b) \quad (4.12)$$

After inverting the eq.(4.8), the dynamic model can be simplified as follow:

$$\ddot{\boldsymbol{\theta}} = (\mathbf{T}^T\mathbf{M}\mathbf{T})^{-1}(-\mathbf{T}^T\mathbf{M}\dot{\mathbf{T}} - \mathbf{T}^T\mathbf{W}\mathbf{M}\mathbf{T})\dot{\boldsymbol{\theta}} + (\mathbf{T}^T\mathbf{M}\mathbf{T})^{-1}\mathbf{T}^T(\mathbf{w}^A + \mathbf{w}^D) \quad (4.13)$$

or alternatively

$$\ddot{\boldsymbol{\theta}} = \mathbf{A}\dot{\boldsymbol{\theta}} + \mathbf{B}(\mathbf{w}^A + \mathbf{w}^D) \quad (4.14)$$

with $\mathbf{A} \equiv (\mathbf{T}^T\mathbf{M}\mathbf{T})^{-1}(-\mathbf{T}^T\mathbf{M}\dot{\mathbf{T}} - \mathbf{T}^T\mathbf{W}\mathbf{M}\mathbf{T})$, $\mathbf{B} \equiv (\mathbf{T}^T\mathbf{M}\mathbf{T})^{-1}\mathbf{T}^T$

4.2 Dissipative Forces

In section 4.1, the location of COM and the amount of dissipative force have been fed to the dynamic model. However, knowing these parameters is not as easy as it seems. In order to calculate the position of COM, the amount of vertical force applied to the platform by each wheel must be known. Moreover, the longitudinal and lateral forces of each wheel applied to the platform must be known to calculate dissipative forces. Longitudinal and lateral forces of caster wheels are purely dissipative force but for driving wheels, it is little different. The lateral forces applied by driving wheels, to their joints in platform, is accounted for none-working constrain forces [27]; but the longitudinal forces applied by driving wheels to the platform are actually pure active forces. These sensed forces, are originated from the torque of driving motors which rolling resistance of the driving wheels has been subtracted from them. By knowing the amount of pure active force from sensors and applied torque to the

driving wheels, the amount of dissipative force of the driving wheels can be calculated as follow:

$$\mathbf{F}_{Dj} \equiv (\tau_j r - F_{hj})\mathbf{h}, \quad i = 1,\ 2 \tag{4.15}$$

where F_{Dj} are the dissipative forces and F_{hj} are longitudinal horizontal forces sensed by force sensors of the driving wheels. This is the main idea behind the closed-loop dynamic model proposed in this thesis.

In order to clarify the proposition of installing dissipative force sensors, a typical model of force sensor and its internal structure is shown in Figure 4.2 [28]. The sensing prob, which is caster wheel and driver wheel in our case, gets installed on the inner frame which is connected to the outer frame via links as shown in Figure 4.2. Otter frame gets installed to a rigid part of the robot body. All sides of the links are covered by strain gauges to measure tension and compression of each side. Knowing the material properties of the internal structure and using homogeneous translation, the applied force and torque to the probe can be calculated. Considering the way that caster wheels get connected to the robot body, the installation bracket shown in Figure 4.3 can play similar role to links in internal structure of force sensors to accommodate strain gauges.

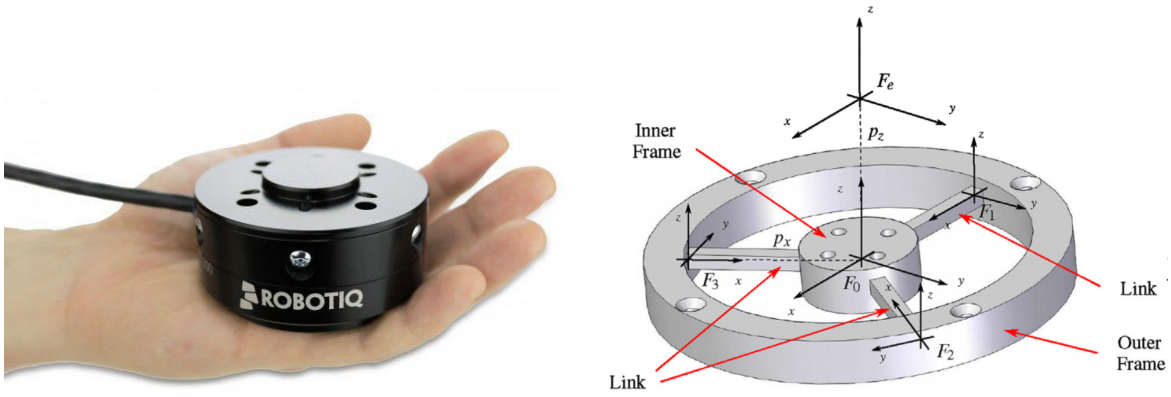

(a) Force sensor (b) Force sensor internal structure

Figure 4.2 A typical force sensor and its internal structure [28]

The driver wheels of the under study robot, are installed directly on robot frame as shown in Figure 4.3. In order to accommodate the strain gauges of force sensors, a simple solution would be to install driver wheel on a separate bracket which itself installed on the robot platform as a link. The design of the proposed bracket is beyond the scope of this study and remains for future work.

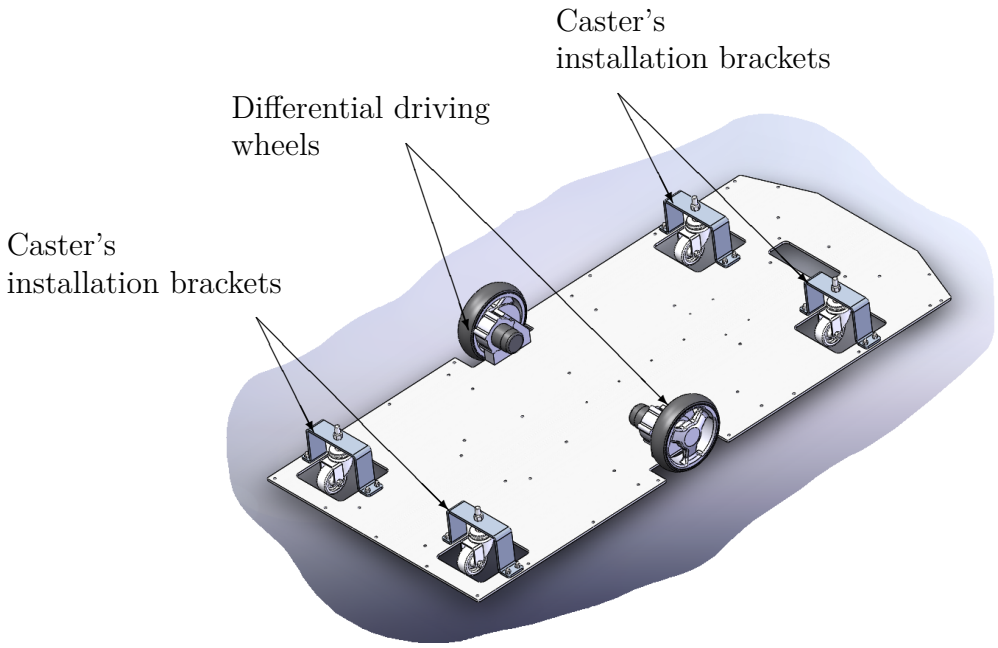

Figure 4.3 Proposed positions to install force sensors

4.3 MATLAB Simscape and Multibody Settings

In order to simulate the interaction between wheels and ground, the MATLAB Simscape contact force library [29] was used. The simulation model of the robot is illustrated in Figure 4.4. The wheel and ground contact was considered as sphere and plane. MATLAB offers linear and non-linear contact force law [30]. The linear law imitate linear spring damper penetration resist force wheres in non-linear law the penetration resist force increase exponentially. In this study, we used linear friction law between wheels and ground which provides a good estimation for non-inflatable tires' forces. [31].

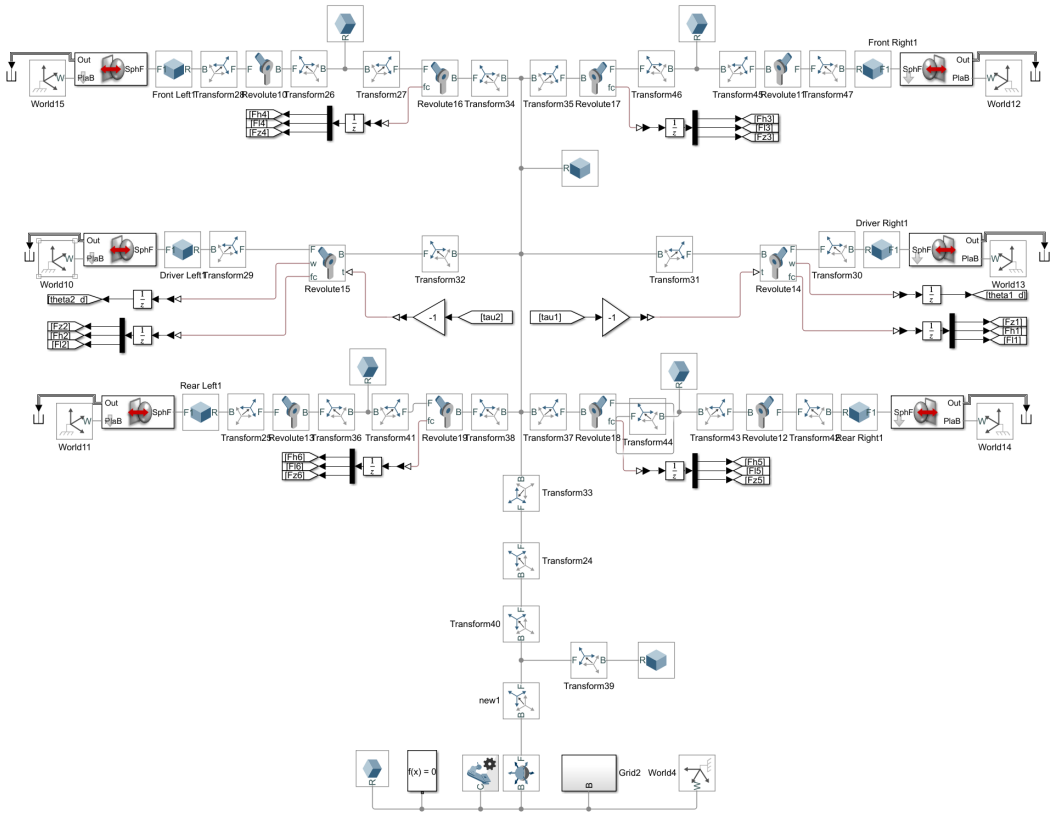

Figure 4.4 Illustration of the robot model in MATLAB Simulink environment using Simscape library.

The friction coefficients of caster wheels and driving wheels are listed in Table 4.2 and Table 4.3 respectively. Although many authors studied the friction model of inflatable tires [26, 32], all friction data of rubber tires, used in AMRs, are not available. So, the data of Table 4.2 and Table 4.3 are approximated from some available data published by well known manufacturers [33, 34].

Table 4.2 Contact parameters for caster wheels and ground

Stiffness (N/m)	$1e^4$
Damping (N/(m/s))	20
Kinetic Friction coefficient	$1e^-1$
Static Friction coefficient	$12e^-2$
Velocity Threshold (m/s)	$1e^-3$

Table 4.3 Contact parameters for driving wheels and ground

Stiffness (N/m)	$1e^3$
Damping (N/(m/s))	10
Kinetic Friction coefficient	$38e^-2$
Static Friction coefficient	$4e^-1$
Velocity Threshold (m/s)	$1e^-3$

In order to validate the usability of this friction data and performance of MATLAB Simscape library in simulation of the wheel ground interaction forces, a simple test was performed. The driving motor of the AMR was actuated for a short amount of time and the longitudinal displacement of the platform was measured as shown in Figure 4.5. As depicted, the robot starts to accelerate at the first 10 seconds, then, by cutting of the input torque, the velocity which is the slop of the plot, decreases gradually over the next 10 seconds. After that, the slop of the plot gets negative which means the wheels rotate backward before start to bouncing. Finally, after a couple of back and forth, the platform gets to equilibrium point and stops completely.

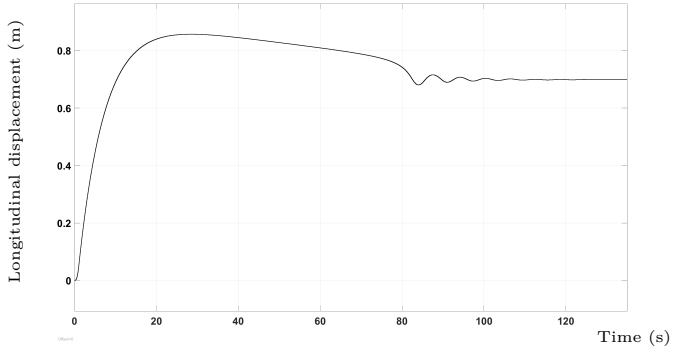

Figure 4.5 Validation of simulation environment considering wheels and ground friction

CHAPTER 5 CONTROL

5.1 Trajectory Tracking

5.1.1 Control Architecture

The kinematic controller regulates AMR's input twist $\dot{\mathbf{q}}_c \equiv [\mathbf{v}_c \ \dot{\phi}_c]^T$to alter the AMR's actual pose $\mathbf{q}_d \equiv [x_d \ y_d \ \phi_d]^T$and robot's actual twist $\dot{\mathbf{q}}_d \equiv [\mathbf{v}_d \ \dot{\phi}_d]^T$ according to the reference pose $\mathbf{q}_r \equiv [x_r \ y_r \ \phi_r]^T$and reference twist $\dot{\mathbf{q}}_r \equiv [\mathbf{v}_r \ \dot{\phi}_r]^T$. The robot's actual pose $\mathbf{q}_d$ and robot's actual twist $\dot{\mathbf{q}}_d$ are read from Navigation System (NS) consist of wheels' encoders and Inertial Measurement Unit (IMU) installed on robot's platform. The origin of the frame $\mathcal{M}$, point o', is the target of trajectory tracking system i.e the aim is to hold it coincidence to the trajectory path. The pose error vector $\mathbf{e}_q \equiv [e_x \ e_y \ e_\phi]^T$ will be defined as follow:

$$\mathbf{e}_q \equiv \begin{bmatrix} e_x \\ e_y \\ e_\phi \end{bmatrix} = \mathbf{q}_r - \mathbf{q}_d = \begin{bmatrix} x_r - x_d \\ y_r - y_d \\ \phi_r - \phi_d \end{bmatrix} \tag{5.1}$$

The deviation in pose $\mathbf{e}_q$ will be adjusted in kinematic level by controlling the robot's twist $\dot{\mathbf{q}}_c$. The twist error vector $\mathbf{e}_{\dot{q}}$ will be defined as follow:

$$\mathbf{e}_{\dot{q}} \equiv \begin{bmatrix} e_v \\ e_{\dot{\phi}} \end{bmatrix} = \dot{\mathbf{q}}_r - \dot{\mathbf{q}}_d = \begin{bmatrix} \mathbf{v}_r - \mathbf{v}_d \\ \dot{\phi}_r - \dot{\phi}_d \end{bmatrix} \tag{5.2}$$

The deviation in twist $\mathbf{e}_{\dot{q}}$ will be regulated in dynamic level using force and twist feedback of the AMR. The control architecture depicted in Figure 5.1 shows the configuration of dynamic and kinematic control layers.

5.1.2 Kinematic Control

Trajectory tracking of the nonholonomic differential drive wheel robot with twist feedback is controlled with a back-stepping method proposed in [13]. In this method, the time derivative of pose error has been considered as follow [13]:

$$\dot{\mathbf{e}}_q = \begin{bmatrix} \dot{e}_x \\ \dot{e}_y \\ \dot{e}_\phi \end{bmatrix} = \begin{bmatrix} \dot{\phi}_d e_y - v_d + v_r \cos e_\phi \\ v_r \sin e_\phi - \dot{\phi}_d e_x \\ \dot{\phi}_r - \dot{\phi}_d \end{bmatrix} \tag{5.3}$$

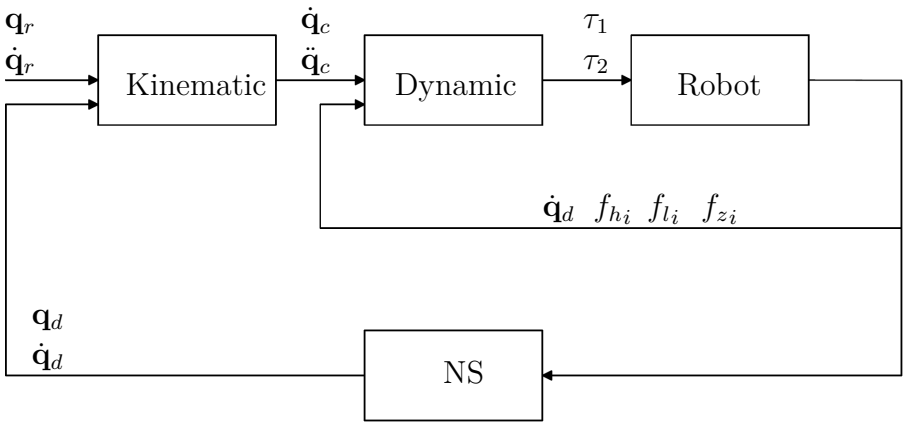

Figure 5.1 The configuration of control system layers

In eq.(5.3) the nonholonomic property of the robot is presenting itself since the three arrays of pose error vectors have to be taken care of with only two inputs of the independent velocity vector. Then, a Lyapanov function defined to make sure the pose error asymptotically converges to zero. As a result, the control law defined the input twist of the robot as :

$$\begin{bmatrix} \mathbf{v}_c \\ \dot{\phi}_c \end{bmatrix} \equiv \begin{bmatrix} k_1 e_x + v_r \cos e_\phi \\ \dot{\phi}_r + k_2 v_r e_y + k_3 v_r \sin e_\phi \end{bmatrix} \tag{5.4}$$

where k_1, k_2 and k_3 are positive real control coefficients which mainly be determined based on trial and error.

5.1.3 Dynamic Control

The dynamic controller is responsible for tracking the desired twist provided by kinematic controller based on the reference twist. In this level, the time-derivative of pose error defined at eq.(5.2) is used to construct sliding surface proposed in [35] as follow:

$$\mathbf{s}(t) = \mathbf{e}_{\dot{q}} + k_4 \int_0^t \mathbf{e}_{\dot{q}}\, dt \tag{5.5}$$

In order to guarantee that the system stays on the sliding surface, the derivative of sliding surface $\dot{\mathbf{s}}(t)$ must be zero when the $\mathbf{s}(t)$=0. The time-derivative of eq.(5.5) can be written as:

$$\dot{\mathbf{e}}_{\dot{q}} + k_4 \mathbf{e}_{\dot{q}} = 0 \quad or \quad \begin{bmatrix} \dot{v}_r \\ \ddot{l}_r \\ \ddot{\phi}_r \end{bmatrix} - \begin{bmatrix} \dot{v}_d \\ \ddot{l}_d \\ \ddot{\phi}_d \end{bmatrix} + k_4 \mathbf{e}_{\dot{q}} = 0 \tag{5.6}$$

Because of the nonholonomic property of the robot, in eq.(5.6), the $\ddot{l}_r$ must be zero, which means we can not demand the robot to have a lateral movement. After taking the time-derivative of eq.(5.5) and using $\mathbf{K}_c$ matrix in equation eq.(3.17) we expect:

$$\begin{bmatrix} \dot{v}_r \\ 0 \\ \ddot{\phi}_r \end{bmatrix} - \mathbf{K}_c \begin{bmatrix} \ddot{\theta}_1 \\ \ddot{\theta}_2 \end{bmatrix} + k_4 \mathbf{e}_{\dot{q}} = 0 \tag{5.7}$$

Using the rule of inverting non square matrix, the inverse of $\mathbf{K}_{3\times 2}$ matrix is given as:

$$\mathbf{K}_{c2\times 3}{}^{-1} = [\mathbf{K}_c \mathbf{K}_c^T]^{-1} \mathbf{K}_c^T \tag{5.8}$$

Applying eq.(4.13) and eq.(5.8) to eq.(5.7), it yields the desired torque of the driving wheels' motors, according to the definition of equivalent control, as:

$$\begin{bmatrix} \tau_1 \\ \tau_2 \end{bmatrix}_{eq} = \mathbf{B}^{-1} \mathbf{K}_c{}^{-1} \ddot{\mathbf{q}}_c + k_4 \mathbf{B}^{-1} \mathbf{K}_c{}^{-1} \mathbf{e}_{\dot{q}} - \mathbf{B}^{-1} \mathbf{B} \mathbf{W}^D - \mathbf{B}^{-1} \mathbf{A} \dot{\boldsymbol{\theta}} \tag{5.9}$$

where, $\ddot{\mathbf{q}}_c$ is the derivative of the robot input twist $\dot{\mathbf{q}}_c$ which is the output of kinematic controller. In [9], the term $\mathbf{B}^{-1}\mathbf{B}\mathbf{W}^D$ has been considered as noise because it is difficult to measure. However, in our case which is carrying a heavy load not necessarily well distributed, the amount of uncertainty caused by the mentioned term is not negligible and instead it is measured by force sensors. The switching control law, which is used to drives the robot during the reaching phase and forces the robots' states to approach the sliding surface, is defined as:

$$\begin{bmatrix} \tau_1 \\ \tau_2 \end{bmatrix}_{sw} = \mathbf{B}^{-1} \mathbf{K}_c{}^{-1} \boldsymbol{\sigma} sign(s) \tag{5.10}$$

Where *sign* is the mathematical sign function and σ is positive definite diagonal matrix as follow:

$$\boldsymbol{\sigma} = \begin{bmatrix} \sigma_1 & 0 \\ 0 & \sigma_2 \end{bmatrix} \quad \sigma_1, \sigma_1 > 0 \tag{5.11}$$

So, the driving wheels output torque is calculated as follow:

$$\begin{bmatrix} \tau_1 \\ \tau_2 \end{bmatrix} = \begin{bmatrix} \tau_1 \\ \tau_2 \end{bmatrix}_{eq} + k_5 \begin{bmatrix} \tau_1 \\ \tau_2 \end{bmatrix}_{sw}, \quad k_5 > 0 \tag{5.12}$$

5.1.4 Fuzzy logic Control

The coefficient k_5 in eq.(5.12) determines the severity of switching behaviour of the control system on the neighbourhood of the sliding surface. In order to force the robot to follow a reference trajectory, the coefficient k_5 must be big enough which consequently causes chattering problem or back and forth between two states with different polarities. In order to eliminate the chattering behaviour of the system, literature [23] have proposed implementation of fuzzy logic control method. Determining the coefficient k_5 proportionally using fuzzy logic, helps to adjust k_5 based on linguistic rules. Lets define velocity tracking error $\mathbf{e}_v$ as the input of the fuzzy logic control method, with range of $[-a_1, a_1]$ where a_1 is the maximum heading velocity of the robot which is 2.5 m/s in our case. The output of the fuzzy system is k_5 which its range was determined by trial and error and in our case it ranges $[0, 20]$. Standard domain of normalized variables $\mathbf{e}_v$ and k_5 are defined as $[-2.5, -2, -1.5, -1, -0.5, 0, 0.5, 1, 1.5, 2, 2.5]$ and $[0, 2, 5, 9, 13]$, respectively, which stand for fuzzy state of qualitative variables as $[NB, NM, NS, ZO, PS, PM, PB]$ and $[ZO, PS, PM, PB]$. The linguistic rules of fuzzy logic control systems are shown in Table.(5.1).

Table 5.1 Fuzzy Logic Controller Linguistic Rules

Abbreviation	Quantitative variables
NB	Negative Big
NM	Negative Medium
NS	Negative Small
ZO	Zero
PS	Positive Small
PM	Positive Medium
PB	Positive Big

The idea behind the fuzzy logic control design is to adjust the switching behaviour pace. When the velocity error $\mathbf{e}_v$ has a large value, the switching behaviour needs to have its maximum value to asymptotically decrease the velocity error. On the other hand, in very small amounts of velocity error, the k_5 must be set as a very small value or zero to avoid chattering problem.

5.2 Simulation and Results

In order to validate the performance of the designed dynamic system, the under study AMR has been simulated in MATLAB Simscape [36]. This MATLAB library gives the advantage of defining the friction between wheels and ground, as a result, the wheel's ground interaction force can be taken into account. The virtual force sensors, in simulation, measure the dissipative forces of caster wheels and active forces of driving wheels which apply to the AMR's base. Furthermore, virtual force sensors can find the location of AMR's COM by reading the vertical load on each wheel.
The performance of the designed controller equipped with force sensors for an AMR with variable center of mass has been simulated and the results compared with the same controller without force sensors. The AMR has been demanded to perform a circular maneuver of 5 m radius with heading velocity of 2 m/s and angular velocity of 1 rad/s. The simulator performed simulation for two different scenarios which are centralized loaded AMR and off-centered loaded AMR. In centralized scenario, the load was placed at the origin of the frame $\mathcal{M}$. In off-centered scenario, the load was placed 200 mm laterally and 400 mm longitudinally far from the origin of the frame $\mathcal{M}$. The control coefficients used for simulation are shown in Table.(5.2).

Table 5.2 Control coefficients used in simulation

k_1	k_2	k_3	k_4	σ_1	σ_2
0.008	0.008	5	19.8	1	1

The Figure 5.2 represents the trajectory tracking, angular velocity, longitudinal velocity and tracking error of an unloaded AMR for both, with and without force sensors. As shown, there is not a disparity between two methods, apparently, when the amount of uncertainty is not huge. The simulation results for an AMR with a 20 kg off-centered load are shown in Figure 5.3. Comparing Figure 5.2 with Figure 5.3 shows, when it comes to a large amount of uncertainty, the trajectory error of the method without force sensors surges 60% in x direction and 48% in y direction; while, this scale for the method with force sensors remains more robust which has only 12.8% and 7% of increase in tracking error along x and y directions respectively. Moreover, regarding the controller without force feedback, in off-centered load scenario, orientation error and angular and heading velocities fluctuate dramatically while for the controller with force feedback, orientation error remains closer to zero and angular and heading velocities follow the references more adequately. It means in off-centered loading

scenario, the adjustment of coefficient k_5 by fuzzy logic control method gets less effective to prevent chattering problem. Furthermore, controller with force feedback has better performance while robot carrying off-centered load regarding the heading velocity since controller without force feedback cannot keep up with the reference velocity. Comparing the heading velocity and angular velocity of two controllers also yields, in case of large amount of uncertainty in AMR's dynamic, the control method without force feedback is not sufficient and a more precise dynamic model needs to be considered using force feedback. More precise dynamic model means the closed loop dynamic model proposed in this study which uses force feedback.

Its worth mentioning, in our study we used true location of the AMR from simulator to compare two methods which is not the case in real world example. Usually, in experiment, the data gathered from driving wheels' encoders and IMU are fused by other control methods such as Extended Kalman Filter [37, 38] to estimate AMR's location. Sensor data are always noisy and consequently there would be some deviation from true location and estimated location which increases the path tracking error accordingly.

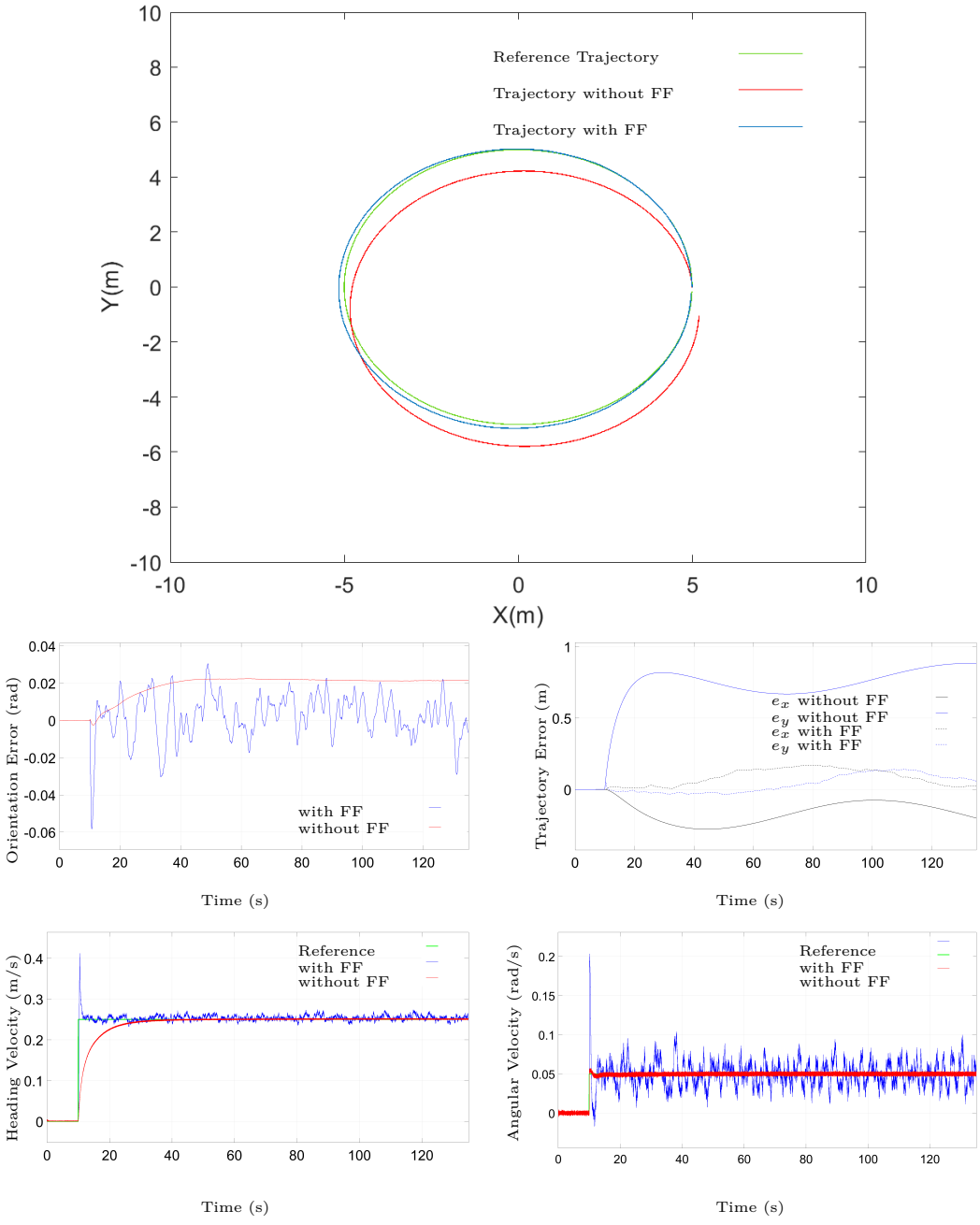

Figure 5.2 Trajectory, trajectory error, orientation error, angular velocity, heading velocity of an unloaded AMR with Force Feedback (FF) and without FF control methods.

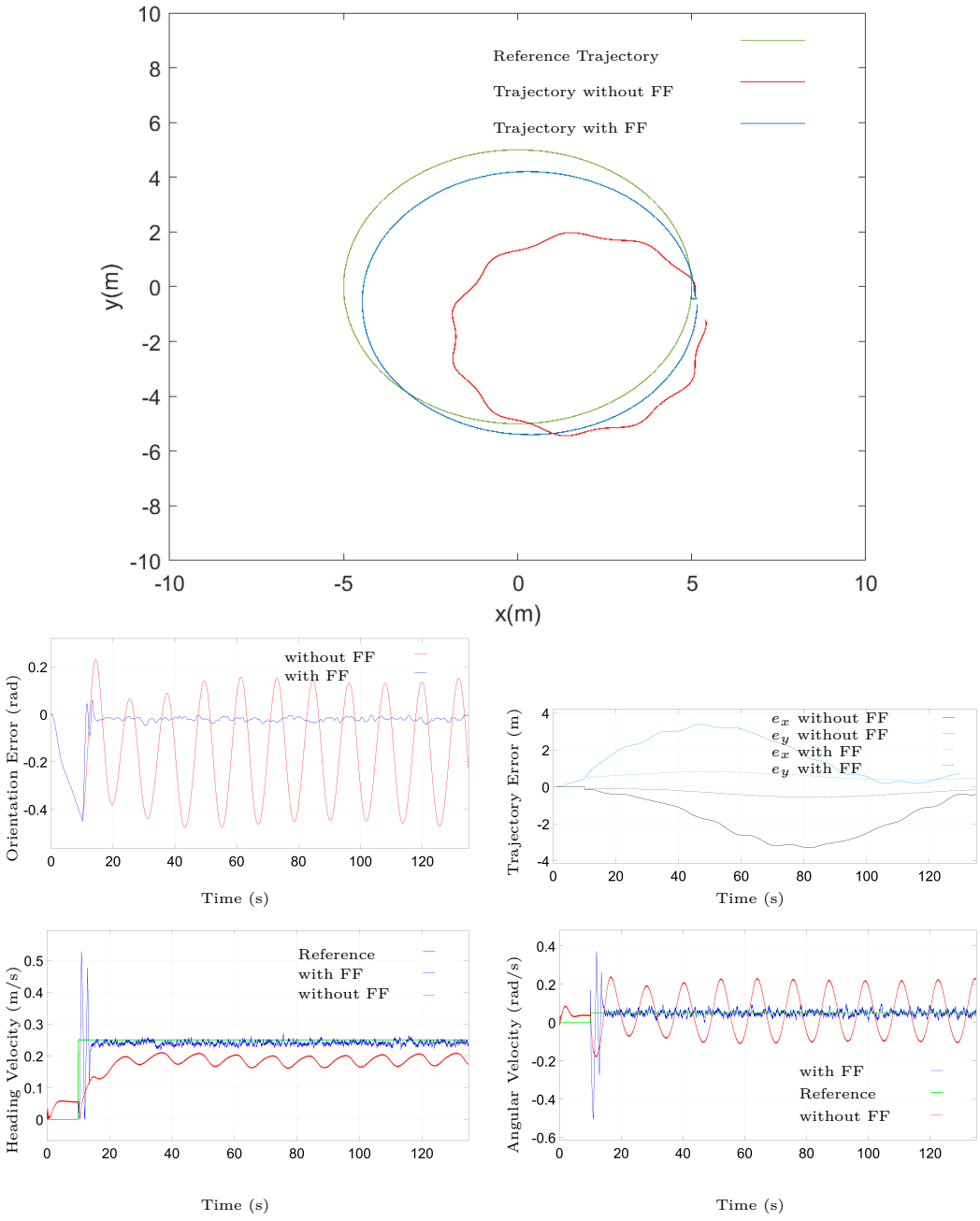

Figure 5.3 Trajectory, trajectory error, orientation error, angular velocity, heading velocity of an off-centered loaded AMR with Force Feedback (FF) and without FF control methods.

CHAPTER 6 GENERAL DISCUSSION

In this chapter the proposed methods are discussed. In this study, a differential drive wheels mobile robot with caster wheels and variable COM has been considered. Unlike the other studies, the location of COM of the under study robot is not fixed and it changes arbitrarily due to the variation in location of load on the robot tray. COM misplacement causes inaccuracy in dynamic model as well as variation in wheel ground interaction forces. The inaccuracy in dynamic model and uncertainty of caster wheels cause path tracking error. Caster wheel is the main source of uncertainty because not only its dissipative force magnitude changes by variation of COM but also the direction of dissipative force varies regarding robot orientation.

For applications such that COM's location considered to be fixed, the relation between caster wheel orientation and robot orientation matters, such as designing wheelchairs [3]. In such applications, the magnitude of dissipative force of caster wheel is a portion of the carrying weight. The orientation of caster wheel calculated in literature [1] helps to find the direction of dissipative force. However, in our study, the magnitude of dissipative forces of caster wheels are unknown, and knowing their orientations does not help.

In order to deal with variation of position of COM, the kinematic model and dynamic model based on an arbitrary position of COM has been derived. Moreover, implementation of force sensor has been proposed to measure the vertical load carried by each wheel and consequently finding the position of COM. Finally, the latest nonlinear control method has been reconsidered to control the new proposed kinematic and dynamic model.

To evaluate the performance of the proposed method, the designed robot model has been imported to MATLAB Simulink environment. The friction between wheels and ground was simulated using MATLAB Simscape contact library to be able to consider the dynamic behavior of wheels and its dissipative forces. At the end, the performance of the proposed method has been compared to one of the latest methods which considers fixed COM. Simulation results show significant improvement in decreasing path tracking error while robot carrying off-centered weight.

CHAPTER 7 CONCLUSION AND RECOMMENDATIONS

7.1 Conclusion

In this study, we considered a free range differential drive wheel mobile robot with variable COM to minimize its path tracking error. To do so, the kinematic of such an AMR was reconsidered based on the location of its instantaneous COM. Also, a new mathematical model was proposed to show how the orientation of caster wheels change by changing the orientation of the robot. Then the dynamic model of the AMR was derived around the location of an arbitrary COM. The interaction forces between wheels and ground are the unknown parameters in the dynamic model. The implementation of force sensors on each wheel has been proposed to determine wheel ground interaction forces of associated wheel and to determine the position of COM of AMR. The robot model with actual size, was simulated in MATLAB simulator using Simscape library to generate friction forces and rolling resistances of wheels. Then, the required control methods where chosen to deal with the nonholonomic properties of the robot. And finally, the path tracking error of the robot with new kinematic model, dynamic model and control method was compared with the other state of the art method in two different scenarios. At the first scenario, the COM of the robot was considered at the middle of the line connecting driver wheels. In the second scenario the location of COM was moved longitudinally and laterally by displacement of the carrying load on the robot tray. In first scenario, the performance of both methods remains almost the same. But, in the second scenario, the new derived model has outstanding performance comparing to the other method. There was a considerable difference between the path tracking error of two methods in second scenario while the orientation error remains almost the same.
In conclusion, the main objective of this study which was to decrease path tracking error of an AMR with variable COM was achieved in simulation level, by reconsidering AMR's kinematic model, dynamic model and implementation of force sensors.

7.2 Recommendation and Future work

The kinematics of the differential drive robot with skidding and slipping has been derived and simplified to the model under the assumption of pure rolling. The reason of such a simplification was the lack of control method to consider slipping and skidding as inputs. Such an input could be received from fused data of Inertia Measurement Unit (IMU) and wheels' encoders. This control method can be derived using advanced nonlinear control

methods such as Back-stepping or sliding mode control. Moreover, the implementation of the used method in the simulation in this thesis was remained to explore.

REFERENCES

[1] M. Montazerijouybari, L. Baron, and S. Kelouwani, "Kinematics of 2-dof agvs with differential driving wheels and caster wheels modeling," in *Symposium on Robot Design, Dynamics and Control*. Springer, 2020, pp. 495–502.

[2] X. Wu, J. Angeles, T. Zou, H. Xiao, W. Li, and P. Lou, "Steering-angle computation for the multibody modelling of differential-driving mobile robots with a caster," *International Journal of Advanced Robotic Systems*, vol. 15, no. 6, p. 1729881418820166, 2018.

[3] F. Chénier, P. Bigras, and R. Aissaoui, "An orientation estimator for the wheelchair's caster wheels," *IEEE Transactions on Control Systems Technology*, vol. 19, no. 6, pp. 1317–1326, 2010.

[4] L. E. Aguilar, T. Hamel, and P. Soueres, "Robust path following control for wheeled robots via sliding mode techniques," in *Proceedings of the 1997 IEEE/RSJ International Conference on Intelligent Robot and Systems. Innovative Robotics for Real-World Applications. IROS'97*, vol. 3. IEEE, 1997, pp. 1389–1395.

[5] P. Soueres, M. Courdesses, S. Fleury *et al.*, "Robust path-following control with exponential stability for mobile robots," in *Proceedings. 1998 IEEE International Conference on Robotics and Automation (Cat. No. 98CH36146)*, vol. 4. IEEE, 1998, pp. 3279–3284.

[6] T. Hamel and D. Meizel, "Robust control laws for wheeled mobile robots," *IFAC Proceedings Volumes*, vol. 29, no. 1, pp. 175–180, 1996.

[7] Z.-P. Jiang and J.-B. Pomet, "Combining backstepping and time-varying techniques for a new set of adaptive controllers," in *Proceedings of 1994 33rd IEEE Conference on Decision and Control*, vol. 3. IEEE, 1994, pp. 2207–2212.

[8] J.-M. Yang and J.-H. Kim, "Sliding mode control for trajectory tracking of nonholonomic wheeled mobile robots," *IEEE Transactions on robotics and automation*, vol. 15, no. 3, pp. 578–587, 1999.

[9] R. Fierro and F. L. Lewis, "Control of a nonholomic mobile robot: Backstepping kinematics into dynamics," *Journal of robotic systems*, vol. 14, no. 3, pp. 149–163, 1997.

[10] T. Yamada, K. Watanabe, K. Kiguchi, and K. Izumi, "Dynamic model and control for a holonomic omnidirectional mobile robot," *Autonomous Robots*, vol. 11, no. 2, pp. 173–189, 2001.

[11] T. Fukao, H. Nakagawa, and N. Adachi, "Adaptive tracking control of a nonholonomic mobile robot," *IEEE transactions on Robotics and Automation*, vol. 16, no. 5, pp. 609–615, 2000.

[12] P. Coelho and U. Nunes, "Path-following control of mobile robots in presence of uncertainties," *IEEE Transactions on Robotics*, vol. 21, no. 2, pp. 252–261, 2005.

[13] Y. Kanayama, Y. Kimura, F. Miyazaki, and T. Noguchi, "A stable tracking control method for an autonomous mobile robot," in *Proceedings., IEEE International Conference on Robotics and Automation.* IEEE, 1990, pp. 384–389.

[14] S. Wang, L. Tao, Q. Chen, J. Na, and X. Ren, "Usde-based sliding mode control for servo mechanisms with unknown system dynamics," *IEEE/ASME Transactions on Mechatronics*, vol. 25, no. 2, pp. 1056–1066, 2020.

[15] R. Solea, A. Filipescu, and U. Nunes, "Sliding-mode control for trajectory-tracking of a wheeled mobile robot in presence of uncertainties," in *2009 7th Asian control conference.* IEEE, 2009, pp. 1701–1706.

[16] J. K. Lee, Y. H. Choi, and J. B. Park, "Sliding mode tracking control of mobile robots with approach angle in cartesian coordinates," *International Journal of Control, Automation and Systems*, vol. 13, no. 3, pp. 718–724, 2015.

[17] F. G. Rossomando, C. Soria, and R. Carelli, "Sliding mode neuro adaptive control in trajectory tracking for mobile robots," *Journal of Intelligent & Robotic Systems*, vol. 74, no. 3, pp. 931–944, 2014.

[18] A. Bessas, A. Benalia, and F. Boudjema, "Integral sliding mode control for trajectory tracking of wheeled mobile robot in presence of uncertainties," *Journal of Control Science and Engineering*, vol. 2016, 2016.

[19] N. Esmaeili, A. Alfi, and H. Khosravi, "Balancing and trajectory tracking of two-wheeled mobile robot using backstepping sliding mode control: design and experiments," *Journal of Intelligent & Robotic Systems*, vol. 87, no. 3, pp. 601–613, 2017.

[20] S. Thanok and M. Parnichkun, "Longitudinal control of an intelligent vehicle using particle swarm optimization based sliding mode control," *Advanced Robotics*, vol. 29, no. 8, pp. 525–543, 2015.

[21] H. Mehrjerdi and M. Saad, "Chattering reduction on the dynamic tracking control of a nonholonomic mobile robot using exponential sliding mode," *Proceedings of the Institution of Mechanical Engineers, Part I: Journal of Systems and Control Engineering*, vol. 225, no. 7, pp. 875–886, 2011.

[22] M. Begnini, D. W. Bertol, and N. A. Martins, "A robust adaptive fuzzy variable structure tracking control for the wheeled mobile robot: Simulation and experimental results," *Control Engineering Practice*, vol. 64, pp. 27–43, 2017.

[23] X. Wu, P. Jin, T. Zou, Z. Qi, H. Xiao, and P. Lou, "Backstepping trajectory tracking based on fuzzy sliding mode control for differential mobile robots," *Journal of Intelligent & Robotic Systems*, vol. 96, no. 1, pp. 109–121, 2019.

[24] N. H. Hadi and K. K. Younus, "Path tracking and backstepping control for a wheeled mobile robot (wmr) in a slipping environment," in *IOP Conference Series: Materials Science and Engineering*, vol. 671, no. 1. IOP Publishing, 2020, p. 012005.

[25] Cyberbotics ltd : Webot an open source and multi-plaform desktop application used to simulate robots, a spin-off of epfl (ecole polytechnique federal de lauzanne), switzerland,. [Online]. Available: https://cyberbotics.com/

[26] R. Rajamani, G. Phanomchoeng, D. Piyabongkarn, and J. Y. Lew, "Algorithms for real-time estimation of individual wheel tire-road friction coefficients," *IEEE/ASME Transactions on Mechatronics*, vol. 17, no. 6, pp. 1183–1195, 2011.

[27] S. K. Saha and J. Angeles, "Dynamics of nonholonomic mechanical systems using a natural orthogonal complement," 1991.

[28] G. Palli, L. Moriello, U. Scarcia, and C. Melchiorri, "Development of an optoelectronic 6-axis force/torque sensor for robotic applications," *Sensors and Actuators A: Physical*, vol. 220, pp. 333–346, 2014.

[29] S. Miller, "Simscape multibody contact forces library," Feb. 2021, [Online; accessed Feb 2021]. [Online]. Available: https://github.com/mathworks/Simscape-Multibody-Contact-Forces-Library/releases/tag/20.2.5.0

[30] "wheel friction force description," https://www.mathworks.com/matlabcentral/mlc-downloads/downloads/submissions/64648/versions/2/previews/CFL_Libs/Libraries/Help/html/Force_Laws.html, accessed: 2021-11-30.

[31] Y.-q. Zhao, L.-g. Zang, Y.-q. Chen, B. Li, and J. Wang, "Non-pneumatic mechanical elastic wheel natural dynamic characteristics and influencing factors," *Journal of Central South University*, vol. 22, no. 5, pp. 1707–1715, 2015.

[32] M. Acosta, S. Kanarachos, and M. Blundell, "Road friction virtual sensing: A review of estimation techniques with emphasis on low excitation approaches," *Applied Sciences*, vol. 7, no. 12, p. 1230, 2017.

[33] "wheel friction description," https://https://www.mhi.org/media/members/14220/130101690137732025.pdf, accessed: 2021-11-30.

[34] "Simscape description," https://www.tyma.eu/pdf/contitech-rotafrix.pdf, accessed: 2021-03-24.

[35] B. S. Park, S. J. Yoo, J. B. Park, and Y. H. Choi, "Adaptive neural sliding mode control of nonholonomic wheeled mobile robots with model uncertainty," *IEEE Transactions on Control Systems Technology*, vol. 17, no. 1, pp. 207–214, 2008.

[36] "Simscape description," https://www.mathworks.com/products/simmechanics.html, accessed: 2021-03-24.

[37] I. Ullah, X. Su, J. Zhu, X. Zhang, D. Choi, and Z. Hou, "Evaluation of localization by extended kalman filter, unscented kalman filter, and particle filter-based techniques," *Wireless Communications and Mobile Computing*, vol. 2020, 2020.

[38] S. Yu and Z. Jiang, "Design of the navigation system through the fusion of imu and wheeled encoders," *Computer Communications*, vol. 160, pp. 730–737, 2020.

APPENDIX A ARTICLE 1: KINEMATICS OF 2-DOF AGVS WITH DIFFERENTIAL DRIVING WHEELS AND CASTER WHEELS MODELING

Mohammadreza Montazerijouybari, Luc Baron, Sousso Kelouwani

Montreal, QC H3T 1J4, Canada
Mohammadreza.Montazerijouybari@polymtl.ca
Luc.Baron@polymtl.ca
Université du Québec à Trois-Rivières
Trois-Rivières QC G8Z 4M3, Canada
Sousso.Kelouwani@uqtr.ca

Status: Published in *Symposium on Robot Design, Dynamics and Control. Springer, Cham, 2020.*

A.1 Abstract

Automatic Guided Vehicle (AGV) are increasingly used in the industry for a wide variety of applications such as goods handling and manufacturing. Under the assumption of no slipping and no skidding, the kinematic model does not involve any geometric parameter of caster wheels. However, when the vehicle is carrying heavy loads, and moreover, not well distributed over the vehicle, the interaction between the caster wheels and the driving wheels become significant, and needed to be taken into account. This paper proposes a mathematical model based on the kinematics in order to predict the behavior of caster wheels. Simulation results show good prediction of caster wheel orientations in some scenarios relative to the dynamic model of the Webots simulator.

A.2 Introduction

Automatic guided vehicles (AGV) are increasingly used in the industry for a wide variety of applications such as goods handling and manufacturing. Several configurations exist for incorporating the motorized driving wheels together with passive wheels, either fixed on the vehicle or free to rotate as implemented by caster wheels. The latter is often included as a passive mean for the stability of the load carried and its inheritance of not affecting the control law, under the assumption of *no slipping* and *no skidding*. However, when carrying heavy

loads, and moreover, not well centered on the vehicle, the interaction between the caster wheels and the driving wheels become significant, and needed to be taken into account. Kinematics and dynamics behavior of differential wheels integrated with caster wheels were well studied in the literature [1–5]. All of them are getting ride of the caster wheel behavior, and hence, are not able to consider this significant interaction with the driving wheels when carrying heavy loads [6]. In this paper, we concentrated on the modeling of the kinematic behavior of caster wheels in order to predict their orientation based only on kinematic means. A long term objective is to incorporate such a mathematical model into control schema of the AGV in order to carry heavy loads not necessarily well centered on the platform. As shown in Fig. A.1, the left and right sides of the platform are symmetric, while the front and rear sides are different. The platform is controlled by two motorized differential driving wheels that are aligned along a common revolute axis. The platform has four passive caster wheels spread over the four corners.

A.3 Problem Formulation

Let us designate points P_i as the pivot points of each caster wheel on the platform, points D_j the contact points of the driving wheels with the ground, while points $O_{\mathcal{A}}$ and $O_{\mathcal{B}}$, respectively, the origins of frames $\mathcal{A}$ fixed to the ground and frame $\mathcal{B}$ attached to the platform. The two independently motorized differential wheels are located along the y-axis of $\mathcal{B}$ and use this axis as a common revolute joints.

A.4 Kinematic Analysis

Under the assumption of *no slipping* and *no skidding* of the wheels, we have a 2-Degree-Of-Freedom (DOF) mobile platform, although it can reaches any position and orientation in the plane, i.e. three unknowns of position and orientation. This under actuation is the fundamental characteristic of a nonholonomic mechanical systems such as wheeled mobile platforms. Since the kinematic formulation is easier expressed in the moving frame $\mathcal{B}$, let us define $\mathbf{i}$, $\mathbf{j}$ and $\mathbf{k}$ as unit vectors along x- , y- and z-axis of frame $\mathcal{B}$, i.e.,

$$\mathbf{i} = [\cos\psi \;\; \sin\psi \;\; 0]^T, \quad \mathbf{j} = [-\sin\psi \;\; \cos\psi \;\; 0]^T, \quad \mathbf{k} = [0 \;\; 0 \;\; 1]^T, \tag{A.1}$$

where ψ is the orientation of the platform. For a planar motion, $\mathbf{k}$ is identical in frames $\mathcal{A}$ and $\mathcal{B}$. The radius of the driving wheels is r_d, while the one of caster wheels is r_c.

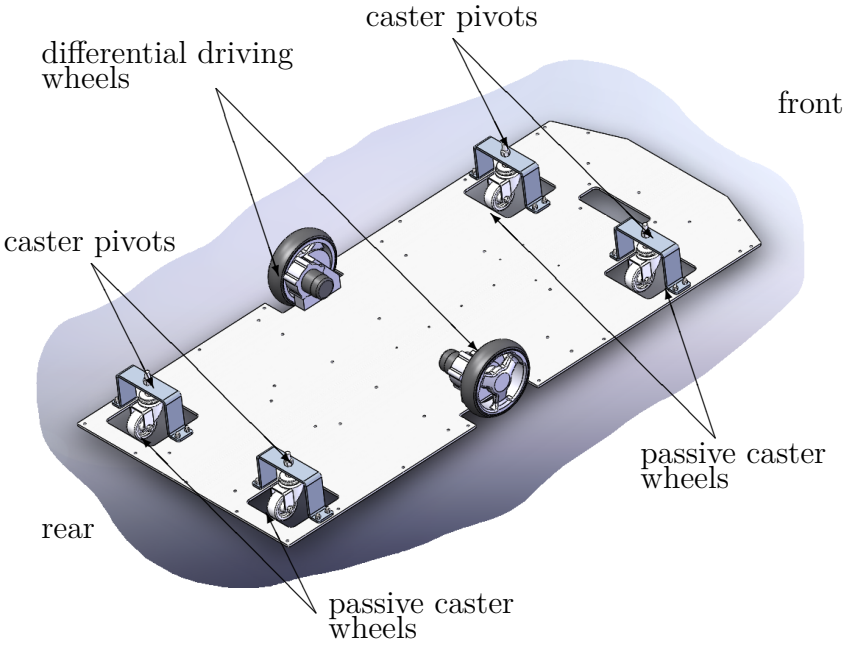

Figure A.1 Automatic Guided Vehicle (AGV) with two motorized differential driving wheels and four passive caster wheels.

A.4.1 AGV Modeling

We follow the kinematic modeling of [7,8] that we summary below for quick reference. The velocity $\mathbf{v}$ of $O_{\mathcal{B}}$ can be written through D_1 as

$$\mathbf{v} = \dot{\mathbf{d}}_1 + \dot{\boldsymbol{\psi}} \times \mathbf{p}_{O_{\mathcal{B}}/D_1} \tag{A.2}$$

where $\dot{\mathbf{d}}_1$ is the velocity of D_1, i.e., the contact point of the driving wheel 1 with the ground, $\mathbf{p}_{O_{\mathcal{B}}/D_1}$ the relative position of $O_{\mathcal{B}}$ with respect to D_1 and $\dot{\boldsymbol{\psi}}$ the angular velocity vector of the AGV, i.e.,

$$\dot{\boldsymbol{\psi}} = \frac{r_d}{2c}(\dot{\theta}_1 - \dot{\theta}_2)\mathbf{k} \tag{A.3}$$

with r_d the radius of the driving wheels and $\dot{\theta}_j$ the actuated revolute speed of the driving wheel j. We can express these vectors in frame $\mathcal{B}$ as

$$\dot{\mathbf{d}}_1 = r_d\dot{\theta}_1\ \mathbf{i}, \quad \mathbf{p}_{C/D_1} = 2c\ \mathbf{j} \tag{A.4}$$

Upon substituting of eqs.(A.3,A.4) into (A.2), it is possible to write the motion of the platform as relationship between the twist $\mathbf{t}$, the actuated driving wheel speeds $\dot{\boldsymbol{\theta}}$ and the *Jacobian* matrix $\mathbf{J}$ as

$$\mathbf{t} \equiv [\dot{\boldsymbol{\psi}}^T\ \mathbf{v}^T]^T = \mathbf{J}\dot{\boldsymbol{\theta}}, \quad \dot{\boldsymbol{\theta}} \equiv [\dot{\theta}_1\ \dot{\theta}_2]^T \tag{A.5}$$

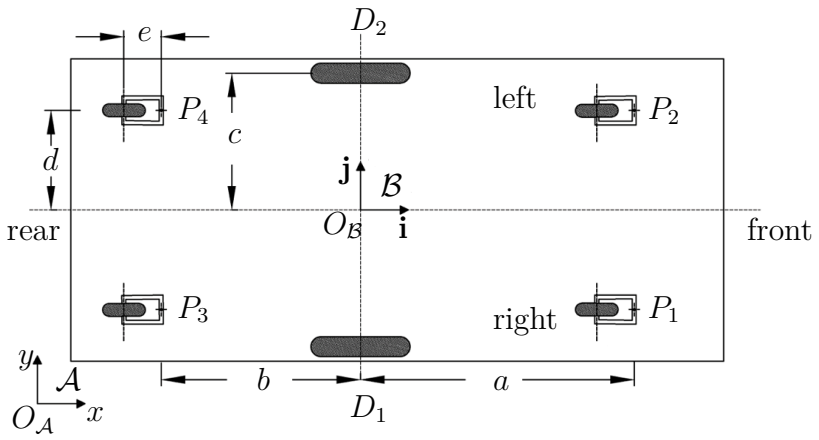

Figure A.2 Geometry of the automatic guided vehicule (AGV) under study

where $\mathbf{t}$ and $\dot{\boldsymbol{\theta}}$ are, respectively, 6- and 2-dimensional columns, and $\mathbf{J}$ is

$$\mathbf{J} = \frac{r_d}{2c} \begin{bmatrix} \mathbf{k} & -\mathbf{k} \\ c\mathbf{i} & c\mathbf{i} \end{bmatrix}_{6\times 2} \tag{A.6}$$

Since the motion is planar, the first two and the last rows of $\mathbf{J}$ are useless, and hence, a reduced formulation is sufficient. Equation (A.5) becomes

$$\mathbf{t}_P = \mathbf{J}_P \dot{\boldsymbol{\theta}}, \tag{A.7}$$

where $\mathbf{t}_P$ and $\mathbf{J}_P$ are, respectively, a 3-dimensional column and a 3×2 matrix, i.e.,

$$\mathbf{t}_P \equiv [\dot{\psi}\ \dot{x}\ \dot{y}]^T, \quad \mathbf{J}_P = \frac{r_d}{2c} \begin{bmatrix} 1 & -1 \\ c\cos\psi & c\cos\psi \\ c\sin\psi & c\sin\psi \end{bmatrix}_{3\times 2} \tag{A.8}$$

Under the assumption of *no slipping* and *no skidding*, eq.(A.7) does not depend on the location of the caster wheels. The kinematic model does not need to take that into account in the kinematic model, and hence, is unable to determine their orientations, as we will be doing next.

A.4.2 Caster Wheel Modeling

Let us consider Fig. A.3 where the vehicle is turning left and rotates around the instantaneous center of rotation (ICR). During any rotation, the ICR remains fixed at point O along the

axis of the driving wheels and intersect the radius $\mathbf{r}_i$ of each caster wheels. The offset of the caster wheels are alway perpendicular to these radius. The orientation of each caster wheel is given by ψ_i.

Start turing

When the vehicle start turning, the velocity of points P_i are pure rotation because Since O is fixed such as

$$\mathbf{v}_{P_i} = r_i\dot{\psi}\begin{bmatrix} \sin(\alpha_i+\psi) \\ \cos(\alpha_i+\psi) \end{bmatrix} \tag{A.9}$$

On the other hand, each caster wheel pivot P_i must rotates around the ICR while the velocity of the contact point to the ground is given by $r_c\dot{\theta}$ along the caster wheel orientation given by ψ_i and the rotation of the caster wheel around the contact point to the ground as $e\dot{\psi}_i$ along the radius $\mathbf{r}_i$ from the ICR. On the other hand, the vehicle rotates around the ICR, we have

$$\mathbf{v}_{P_i} = \begin{bmatrix} r_c\dot{\theta}_i\cos\psi_i - e\dot{\psi}_i\sin\psi_i \\ r_c\dot{\theta}_i\sin\psi_i + e\dot{\psi}_i\cos\psi_i \end{bmatrix} \tag{A.10}$$

Once comparing eqs. (A.9) and (A.10), we get

$$\tan\psi_i = \frac{r_i\dot{\psi}\cos(\alpha_i+\psi) - e\dot{\psi}_i\cos\psi_i}{r_i\sin(\alpha_i+\psi) + e\dot{\psi}_i\sin\psi_i} \tag{A.11}$$

When the vehicle start turning, an ICR moves instantly along the driving wheel axis at distance r, as shown in Fig. A.3. From the other geometry of the platform, we can compute the final orientation of each caster wheel $[\psi_i]_f$ as

$$[\psi_i]_f = \frac{\pi}{2} - \psi - \alpha_i, \tag{A.12}$$

with

$$\alpha_1 = \tan^{-1}(\frac{r+d}{a}), \quad \alpha_2 = \tan^{-1}(\frac{r-d}{a}), \tag{A.13}$$

$$\alpha_3 = \tan^{-1}(\frac{r+d}{b}), \quad \alpha_4 = \tan^{-1}(\frac{r-d}{b}), \tag{A.14}$$

Start going straight

When the vehicle start going straight forward after turning its caster wheels are not yet in neutral orientation, but will do so with a kinematic relationship. As shown in Fig. A.3, each

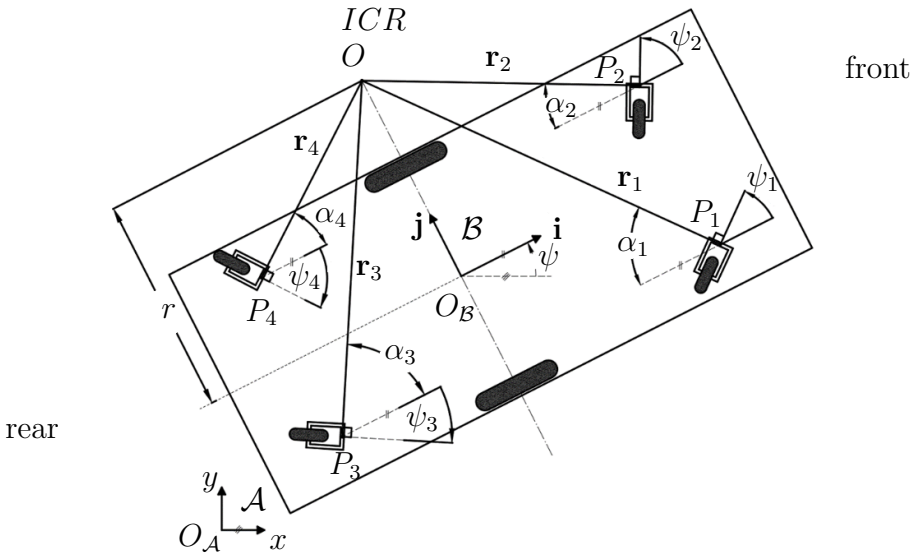

Figure A.3 Caster wheels orientations relative to the instantenious center of rotation (ICR)

caster wheel pivot P_i must follow the vehicle, while the velocity of the contact point to the ground is given by $r_c\dot{\theta}$ along the caster wheel orientation given by ψ_i and the rotation of the caster wheel around the contact point to the ground as $e\dot{\psi}_i$ along the radius $\mathbf{r}_i$ from the ICR. Since the sum of these two vectors must results in the velocity $r_d\dot{\theta}$ of the vehicle as

$$\text{Along } \mathbf{i} \quad : \quad r_d\dot{\theta} = r_c\dot{\theta}_i\cos\psi_i + e\dot{\psi}_i\sin\psi_i \tag{A.15}$$

$$\text{Along } \mathbf{j} \quad : \quad e\dot{\psi}_i\cos\psi_i = r_c\dot{\theta}_i\sin\psi_i \tag{A.16}$$

Upon substitution of eq.(A.16) into (A.15) in order to get ride of $\dot{\theta}_i$, we obtain

$$\frac{r_d\dot{\theta}}{e} = \dot{\psi}_i(\frac{1}{\sin\psi_i} + \sin\psi_i) \tag{A.17}$$

while the second term of the right-hand-side is neglected. The integral relative to time of eq.(A.17) between the initial conditions ψ_i and the final condition $[\psi_i]_f$, we have

$$\int \frac{r_d\dot{\theta}}{e} = \int_{\psi_i}^{[\psi_i]_f} \frac{\dot{\psi}_i}{\sin\psi_i} \tag{A.18}$$

$$\frac{r_d\theta}{e} = \ln[\tan([\psi_i]_f/2)] - \ln[\tan(\psi_i/2)] \tag{A.19}$$

A.5 Simulation Results

The mathematical model of eqs(A.12) and (A.19), for determining the caster wheel finale orientation ψ_i, is compared with the dynamic simulation of the Webot platform [x] along two different scenarios. Dimensions used in simulations are shown in Table A.1. In scenario 1, the platform is going straight forward and start turning with two different radius. We select for an easy interpretation such as a) having an ICR at point $O_{\mathcal{B}}$ so turning around itself ($r = 0mm$); b) having an ICR at point D_j so that the platform turns around one of its driving wheel ($r = 344mm$). In scenario 2, the platform is turning with two different radius and start going straight forward c) from $r = 0mm$; and d) from $r = 344mm$. Apparently from Fig. A.4, the mathematical model is a rather coarse in scenario 1, while behaving better in scenario 2. However, we don't have much information about the elements included into the dynamic model of Webot [9].

A.6 Conclusions

We have presented a new mathematical model base on kinematics in order to predict the behavior of caster wheels, and more specifically its orientation for two simple scenarios. First, start turning by a known radius or stop turning and going straight forward. The mathematical model is able to capture the main behavior of the motion, but still other approaches remains to explore in order to have a simple prediction of the reaction of caster wheels. The validity of mathematical model has been verified by running the full model of AGV in simulation environment using Webot environment.

Table A.1 Geometrical dimensions of the AGV used in simulation (mm)

a	b	c	d	e	r_c	r_d
631	562	344	250	34	38	100

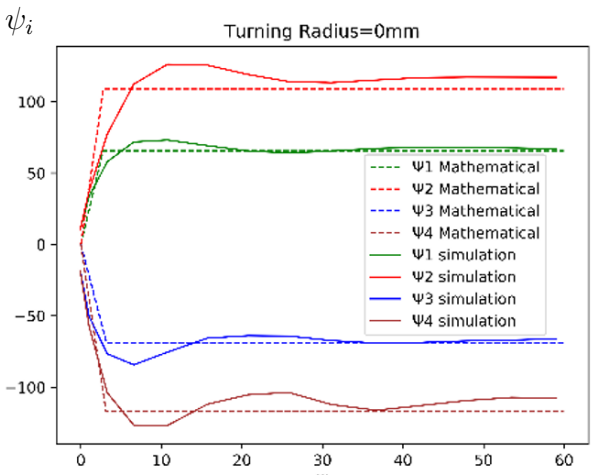

(a) start turning at $r = 0\ mm$;

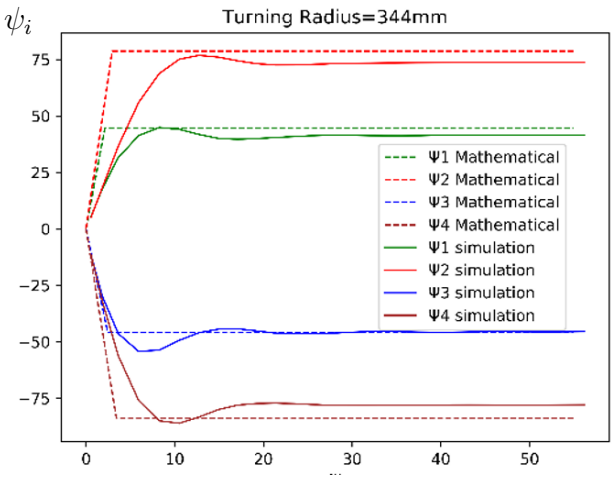

(b) start turning at $r = 344\ mm$;

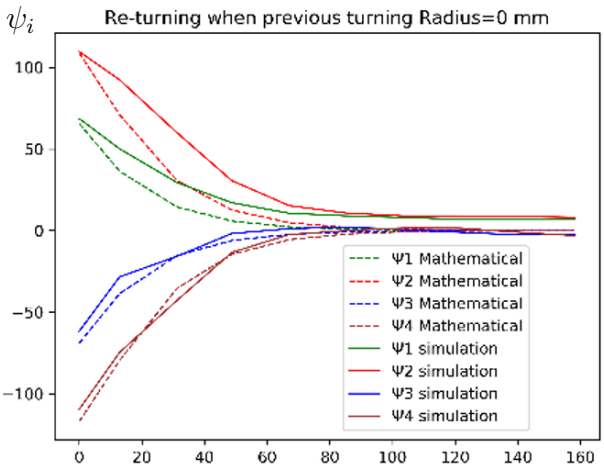

(c) straight from a $r = 0\ mm$;

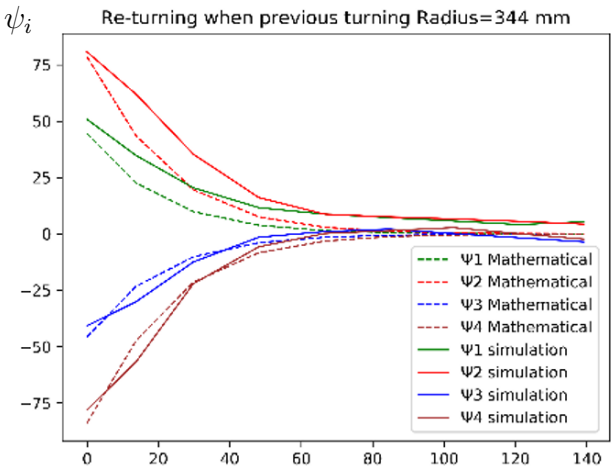

(d) straight from a $r = 344\ mm$;

Figure A.4 Mathematical model and Webot's dynamic simulation : scenario 1 from the neutral orientation of the caster wheels a) turning with $r = 0\ mm$; b) turning with $r = 344\ mm$; scenario 2 going straight forward c) from a turning of $r = 0\ mm$; and d) from turning of $r = 344\ mm$.

REFERENCES

[1] Gentile, A.,Messina, A., Trentadue, A.: Dynamic Behavior of a Mobile Robot Vehicle with a two Caster and two driving Wheel Configuration. Vehicle System Dynamics **25**(2), pp. 89–112 (1996). 10.1080/00423119608968959

[2] Chen, P.-C., Huang, H.-P.: T3D Dynamical Analysis for a Caster Wheeled Mobile Robot Moving on the Frictional Surface. In: IEEE/RSJ Int. Conference on Intelligent Robots and Systems, October 2006, Beijing, China (2006). 10.1109/IROS.2006.282244

[3] Angeles, J.: Fundamentals of Robotic Mechanical Systems : Theory, Methods, and Algorithms. 2nd edn. Springer, (2003)

[4] Kulkarni, A.V.: Instant Center Based Kinematic and Dynamic Motion Synthesis for Planar Mobile Platforms. PhD thesis, University of Texas (2009)

[5] Zaw, M.T.: Kinematic And Dynamic Analysis of Mobile Robot. M.Sc. thesis, National University of Singapore (2003)

[6] Naraghi, M.: Dynamics and Control of Fast Automated Guided Vehicles for High Load Applications. PhD thesis, University of Ottawa (1996)

[7] Saha, S., Angeles, J.: Kinematics and Dynamics of a Three-Wheeled 2-DOF AGV. In IEEE Proceedings, 1989 Int. Conference on Robotics and Automation, Scottsdale, AZ (1989).10.1109/ROBOT.1989.100202

[8] Saha, S., Angeles, J., Darcovich, J.: The Kinematic Design of a 3-dof Isotropic Mobile Robot. In Proceedings IEEE International Conference on Robotics and Automation, (1993). 10.1109/ROBOT.1993.291996

[9] Cyberbotics Ltd : WEBOT an open source and multi-plaform desktop application used to simulate robots, A spin-off of EPFL (Ecole Polytechnique Federal de Lauzanne), Switzerland, `https://cyberbotics.com/`. Last accessed Febuary 2020.